© Copyright by Shyam Janakiraman 2014
All Rights Reserved

AN ADAPTIVE SENSORLESS CONTROL FOR MAXIMUM POWER POINT TRACKING IN WIND ENERGY CONVERSION SYSTEM

A Thesis

Presented to

the Faculty of the Department of Electrical and Computer Engineering

University of Houston

In Partial Fulfillment

of the Requirements for the Degree

Master of Science

in Electrical Engineering

by

Shyam Janakiraman

May 2014

AN ADAPTIVE SENSORLESS CONTROL FOR MAXIMUM POWER POINT TRACKING IN WIND ENERGY CONVERSION SYSTEM

Shyam Janakiraman

Approved:

Chair of the Committee
Dr. Wajiha Shireen
Professor
Electrical and Computer Engineering

Committee Members:

Dr. E. J. Charlson
Professor
Electrical and Computer Engineering

Dr. Robert Provence
Aerospace Engineer
NASA, Johnson Space Center

Suresh K. Khator, Associate Dean
Cullen College of Engineering

Badri Roysam, Professor and Chair
Electrical and Computer Engineering

Acknowledgements

First and foremost I offer my sincerest gratitude to my advisor, Dr. Wajiha Shireen, who has supported me thoughout my thesis with her patience and knowledge whilst allowing me the room to work in my own way. Without her encouragement and effort this thesis would not have been completed or written.

I thank Dr. E J Charlson and Dr. Robert Provence, for serving on my thesis committee. I would also like to thank my labmates, Radhakrishna Kotti and Preetham Goli for all their support, guidance and encouragement.

Lastly, I thank my parents and God for always being with me.

AN ADAPTIVE SENSORLESS CONTROL FOR MAXIMUM POWER POINT TRACKING IN WIND ENERGY CONVERSION SYSTEM

An Abstract

of a

Thesis

Presented to

the Faculty of the Department of Electrical and Computer Engineering

University of Houston

In Partial Fulfillment

of the Requirements for the Degree

Master of Science

in Electrical Engineering

by

Shyam Janakiraman

May 2014

Abstract

This thesis presents a novel mechanical sensorless adaptive control algorithm for Maximum Power Point Tracking (MPPT) in Wind Energy Conversion Systems (WECS). The proposed control algorithm allows the generator to track the optimal operation points of the wind turbine system under fluctuating wind conditions using an efficient two-step process. This algorithm does not require the knowledge of turbine mechanical characteristics such as its power coefficient curve, power or torque characteristic. The proposed control algorithm is simulated in PSCAD/EMTDC. This thesis also aims at designing a scaled laboratory prototype that is necessary to replicate the characteristics of a wind turbine for any wind speed in a controlled test environment without depending on natural wind resources and actual wind turbine. The Wind Turbine Test Bench System (WTTBS) uses an induction motor as a prime mover to replicate the behavior of a wind turbine shaft. The brain of WTTBS is a Digital Signal Processor (DSP) based algorithm which controls the motor. The simulations for the test bench system were carried out in MATLAB/SIMULINK and PSCAD/EMTDC. Test bench system is prototyped using a TI TMS320F28069M.

Table of Contents

List of Figures

List of Tables

Chapter 1 Introduction

Wind power is an affordable, efficient and abundant source of domestic electricity. It is pollution-free and cost-competitive in comparison to the energy from new coal and gas-fired power plants in many regions. The wind industry has been growing rapidly in recent years. In 2011 alone, 3464 turbines went up across the United States, and today, American wind generates enough electricity to power more than 11 million homes [1]. However, due to wind's highly erratic nature, an intelligent control strategy must be implemented to harvest as much potential wind energy as possible while it is available. Because of the merits, and recent technological advancements in wind turbine aerodynamics and power electronic interfaces, wind energy is considered to be an excellent supplementary energy source. Research to extract the maximum power out of the available wind energy is an essential part of making wind energy much more viable and attractive.

1.1 Advantages Of Wind Energy

(1) Wind energy produces no polluting emissions of any kind, including those that cause global warming.

(2) Wind turbines use a fuel that is free, inexhaustible and immune from the drastic price swings to which fossil fuels are subject.

(3) With careful siting and outreach to the local community, wind farms can be built in a fraction of the time it takes to construct coal or natural-gas power plants. A 50-megawatt wind farm can be completed in less than a year.

(4) When installed at the right location, it takes only three to eight months for a wind energy farm to recoup the energy consumed by its building and instal-

lation, one of the fastest "energy payback times" of any energy technology on the market.

(5) Wind power consumes no water during operation. This will be an increasingly important attribute as the water-energy nexus grows in importance and as water use becomes an increasingly important facet of defining sustainability.

1.2 Wind Energy Market

Wind power in the United States is expanding quickly over the last several years. Construction of new wind power generation capacity in the fourth quarter of 2012 totaled 8380 megawatts (MW) bringing the cumulative installed capacity to 60,007 MW as shown in Fig 1.1. As of the end of 2013 the total generating capacity of wind power is about 61,108 MW [2]. Wind generation also has a record 12,000 MW under construction including 10,900 MW that began construction in the 4th quarter of 2013. Texas has over 7,000 MW under construction. This capacity is exceeded only by China.

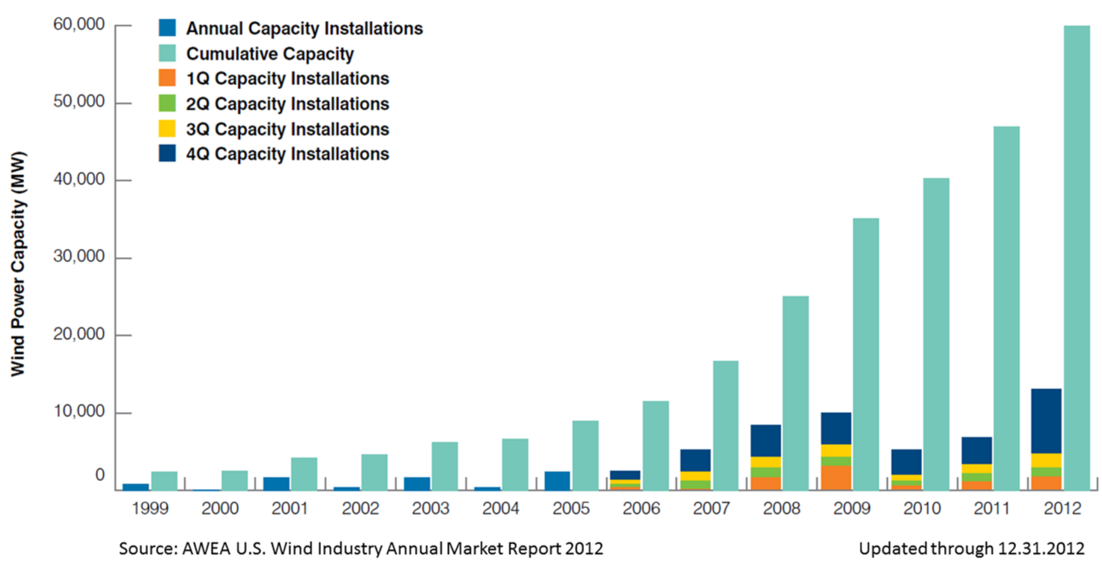

Figure 1.1. Wind Statistics

However, according to the US Energy Information Administration (EIA), the US leads the world in produced electricity from wind, 120 billion kW-hr in 2011, versus 73 billion kW-hours for China. Sixteen states have installed over 1,000 MW of wind capacity with Michigan just breaking the mark in the 4th quarter of 2013, also a total of 39 states and Puerto Rico now have installed at least some utility-scale wind power. Texas, with 12,355 MW of capacity, has the most installed wind power capacity of any U.S. state, followed by California and Iowa with 5,830 MW and 5,178 MW respectively [3].

1.3 Wind Energy Conversion Principles

1.3.1 Background

Energy available in wind is basically the kinetic energy of large masses of air moving over the earth's surface. Blades of the wind turbine receive this kinetic energy, which is then transformed to mechanical or electrical forms, depending on the end use. The efficiency of converting wind to other useful energy forms greatly depends on the efficiency with which the rotor interacts with the wind stream [4].

1.3.2 Air Power

The natural motion of air in the atmosphere, wind, is caused by pressure differences across the surface of the earth due to the uneven heating via solar radiation. From studies of fluid mechanics, this flow of air can be analyzed as mass flow given by

$$\frac{dm}{dt} = \rho A v \ , \tag{1.1}$$

where m is the mass of air in the considered volume , A is the area of incident air stream, v and ρ are the velocity and density of flow respectively. Therefore, the kinetic energy available in the wind is given by

$$E_{air} = \frac{1}{2} m v^2 \, . \tag{1.2}$$

The rate of change of energy gives us the total power stored in the wind

$$P_{air} = \frac{1}{2} \rho A v^3 \, . \tag{1.3}$$

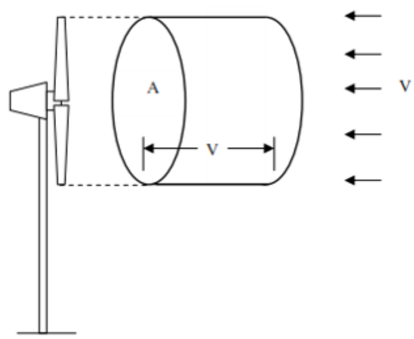

Figure 1.2. Flow of air as Mass flow

Generally A, area of incident air stream, is taken as the area swept by Wind Energy Conversion Systems (WECS). Such systems convert the linear momentum of the air stream into a rotation of the WECS rotor, with a maximum possible efficiency of 59.26%, referred to as Betz limit [5]

1.3.3 Kinetic energy to Mechanical energy conversion

The theoretical power available in wind is established by Eqn.(1.3), but the power extracted from the wind turbine depends on the efficiency of the wind turbine. The aerodynamic efficiency of the turbine while converting wind into usable mechanical turbine power is described by its power coefficient, Cp, curve. The physical meaning of the Cp curve is the ratio of the actual power delivered by the turbine and the theoretical power available in the wind. A turbine's efficiency, and thus power coefficient curve, is what differentiates one turbine from another [6].

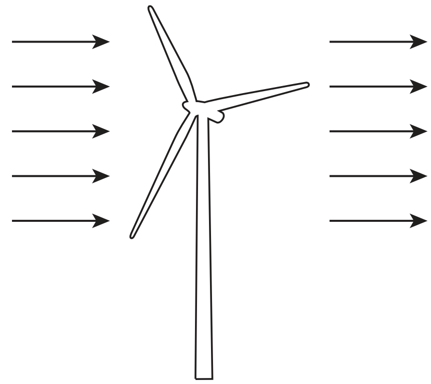

Figure 1.3. Betz Law

For example, if the wind turbine converts 70% of the Betz Limit into electricity ,then the C_p of this wind turbine would be 0.7 x 0.59 = 0.41. So this wind turbine converts 41% of the available wind energy into mechanical power. This is actually a pretty good coefficient of power. Good wind turbines generally have C_p of 0.35-0.45 range.

1.3.4 Factor effecting wind power

From Eqn.(1.3) it can be seen that power extracted by the wind is directly proportional to cube of the wind speed. So at higher windspeeds, the power in the wind turbine is high. Also, since the power is proportional to the rotor swept area, and thus to the square of the diameter, doubling the rotor diameter will quadruple the available power. Air density also plays a role in the amount of available mechanical power of the turbine; lower air densities (e.g. warm air) results in less available power in wind. The power coefficient function, C_p, is dependent on two factors: i) the tip speed ratio (λ) and ii) the pitch angle (β) as shown in Fig 1.4. This function is normally provided by the wind turbine manufacturer since it characterizes the efficiency of the wind turbines.

The Tip Speed ratio (λ) is the ratio of turbine angular speed and windspeed

($\lambda = \frac{\omega_{turb} R}{V}$) [7]. The pitch angle, β refers to the angle at which the turbine blades are aligned with respect to its longitudinal axis. The pitch angle of the blades can be controlled in such a way that the maximum mechanical power from the wind is extracted. For example, if the wind velocity exceeds the rated windspeed of the system, then the rotor blades would be pitched (angled) out of the wind, and when the windspeed

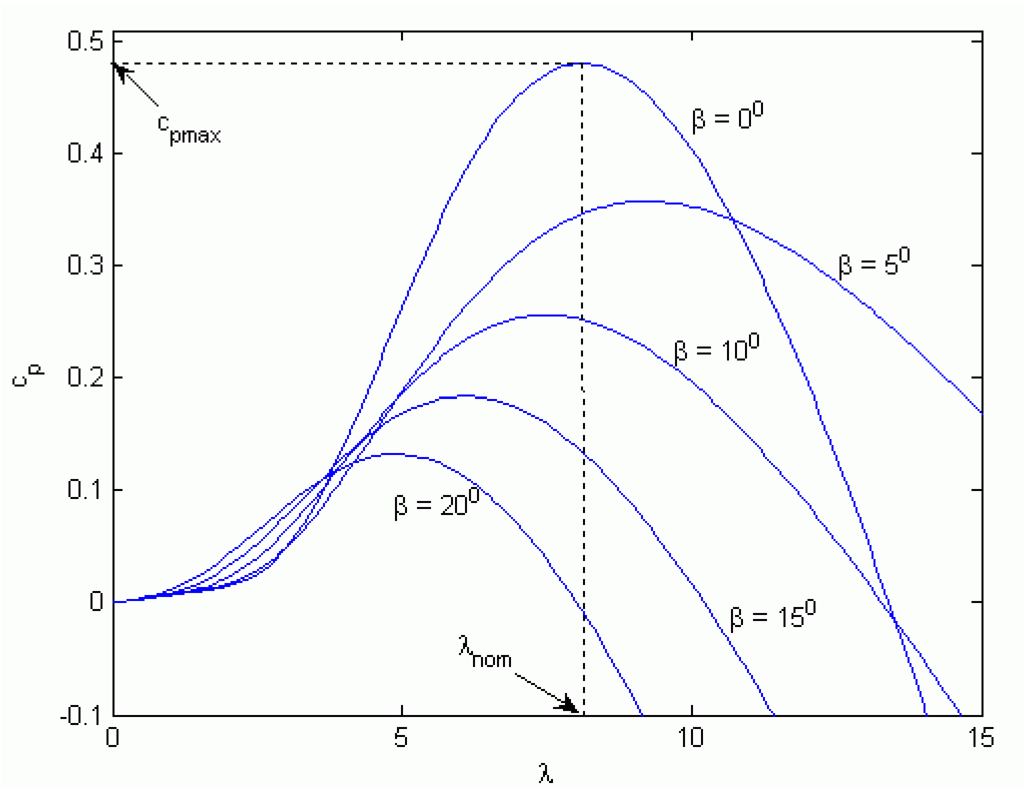

Figure 1.4. Variation of C_p of a windturbine for various β

is below that of the rated value, the rotor blades are pitched back into the wind [8]. This mechanism is implemented by means of hydraulic systems. In the systems where the variable pitch control is not implemented, the C_p functions for those wind turbines depend only on the tip speed ratio.

Since the air density and rotor swept area in Eqn.(1.4) can be considered constant, the power curves for each wind speed are only influenced by the C_p curve.

Thus, the shape of the power characteristic is similar to the C_p curves as shown in Fig 1.4.

1.3.5 Power and Torque Characteristics

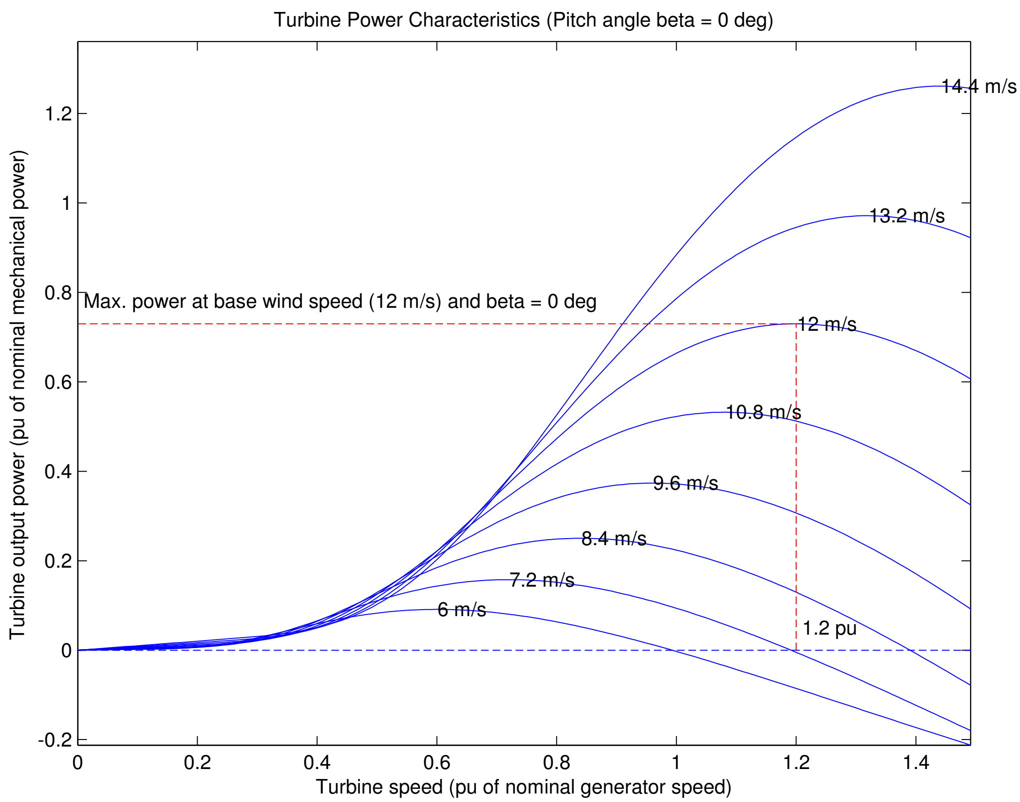

Figure 1.5. Power characteristics of a wind turbine

The mechanical turbine power is given by

$$P_m = \frac{1}{2}\rho C_p(\lambda, \beta) A v^3 m \ , \tag{1.4}$$

where $\lambda = \frac{\omega_{turb} R}{v}$, is called the tip speed ratio and C_p is the power coefficient which determines the efficiency of the wind turbine. The Power characteristics of a wind turbine a range of wind speeds is shown in Fig 1.5. The mechanical torque developed by the wind turbine is

$$T_m = \frac{1}{2}\rho C_p(\lambda, \beta) A v^3 \frac{1}{\omega_{turb}} \,. \tag{1.5}$$

A generic equation is used to model $C_p(\lambda, \beta)$ based on the turbine modeling characteristics [9] is:

$$C_p(\lambda, \beta) = C_1(\frac{C_2}{\lambda_i} - C_3\beta - C_4)e^{-\frac{C_5}{\lambda_i}} + C_6\lambda \tag{1.6}$$

with

$$\frac{1}{\lambda_i} = \frac{1}{\lambda + 0.08\beta} - \frac{0.035}{\beta^3 + 1} \,. \tag{1.7}$$

The coefficients C_1 to C_6 are: C_1 = 0.5176, C_2 = 116, C_3 = 0.4, C_4 = 5, C_5 = 21 and C_6 = 0.0068.

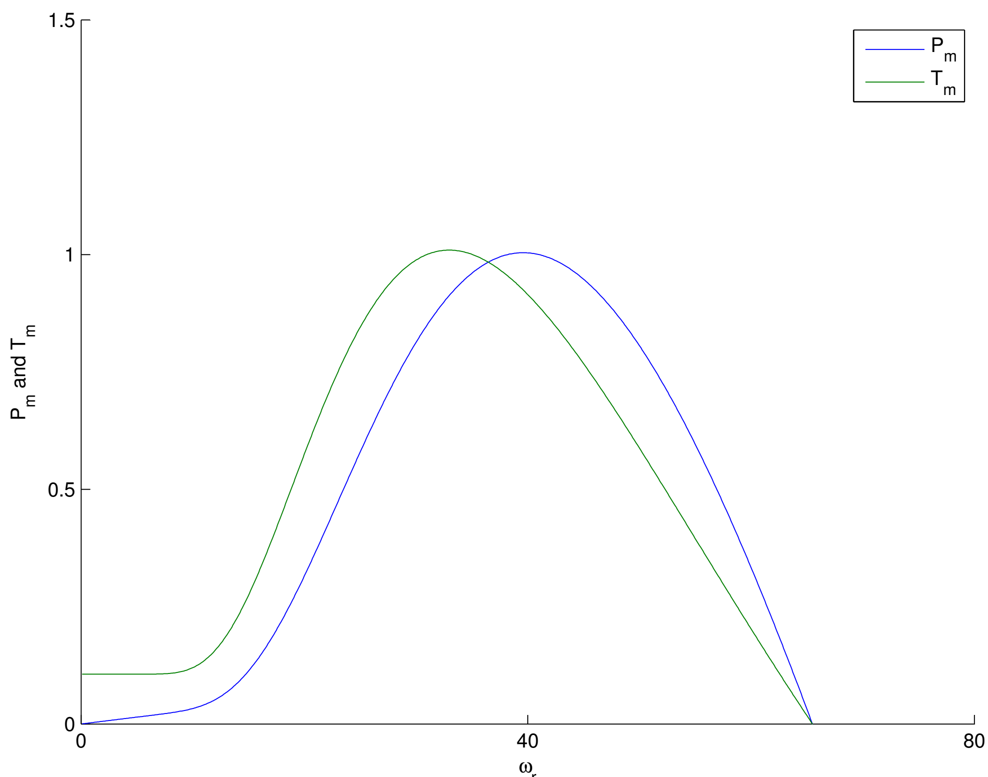

Figure 1.6. Power characteristics vs Torque characteristics for a windspeed

As seen from Eqn.(1.5) the torque is the mechanical power divided by the angular speed of the turbine, the shape of the curve is very similar to the power curve.

However, their peaks do not correspond to the same rotor speed. Therefore, the rotor speed that gives maximum torque does not correspond to the rotor speed that gives maximum as shown in Fig 1.6.

1.4 Concept of Maximum Power Point

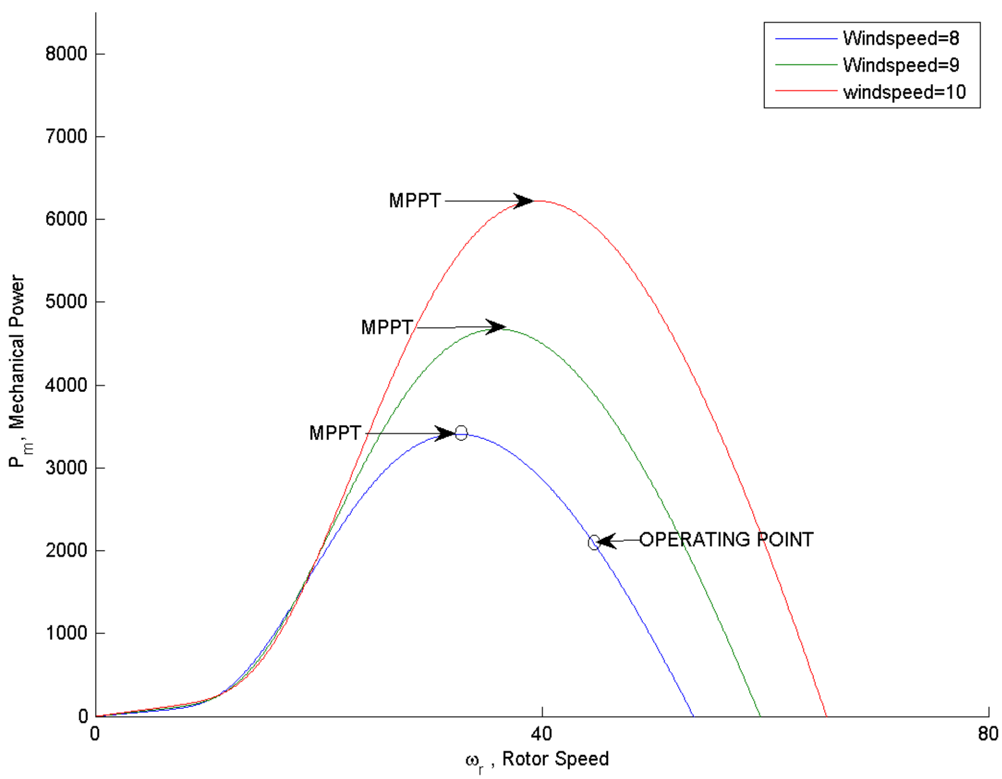

Figure 1.7. Various MPP for a turbine under various wind conditions

Wind energy, even though abundant, varies continually as wind speed changes throughout the day. The amount of power output from a wind energy conversion system (WECS) depends upon the accuracy with which the peak power points are tracked by the maximum power point tracking (MPPT) controller of the WECS control system irrespective of the type of generator used. From Fig 1.7, it can be noted that for every wind speed there is a unique rotor speed for which the power curve attains its maximum. A small variation in the rotor speed will drastically change the power owing to the aerodynamic model of the wind turbine. Turbines usually do not operate at the optimum turbine speed for any given wind velocity because of the effects of generator loading and windspeed fluctuations. Hence, a large percentage of wind power goes wasted.

MPPT algorithms are implemented to increase the efficiency of the system and to make it cost effective. Same rotor speed for different windspeed will fetch us different power due to C_p function. $C_{p,max}$ for a fixed pitched wind turbine corresponds to one particular TSR value. Because the TSR is a ratio of the wind speed and the turbine angular rotational speed, the optimum speed for maximum power extraction is different for each wind speed but the optimum TSR value remains a constant value. Fixed-speed wind turbine systems will only operate at its optimum point for one wind speed [10].

So to maximize the amount of power captured by the turbine, variable-speed wind turbine systems are used because they allow turbine speed variation [6] [11]. Power extraction strategies assesses the wind conditions and then forces the system to adjust the turbine's rotational speed through power electronic control and mechanical devices so that it will operate at the turbine's highest aerodynamic efficiency. The primary challenge of wind energy systems is to be able to capture as much energy as possible from the wind in the shortest time. From the electronics point of view, this goal can be achieved through different converter topologies and maximum power point tracking (MPPT) algorithms.

1.5 Concept of Proposed Algorithm

Out of various MPPT algorithms researched so far, Hill climbing search(HCS) method proves to be the method that is system independent, ie., it doesn't require any prior information about the system, turbine and generator characteristics. Hence, HCS is the ideal choice for a MPPT. However HCS has few serious problems such as speed efficiency trade off and wrong directionality under rapid wind change [12]. There have been few researches in the past that have solved wrong directionality problem by using an optimum perturbation size [13]. Authors of [14] [15] suggested a solution on the speed efficiency trade-off problem, proposing a variable-step hill climbing governed by the magnitude of the derivative of power P with respect to a control variable such as the duty ratio D of the MPPT converter. But none of these provide a complete solution for both the problems. This thesis presents a very simple and effective solution to the two basic problems of HCS by making use of the general characteristic of the optimal power curve. The non uniqueness of the optimal curve is taken care by a novel scanning process.

1.6 DC-DC Boost Chopper

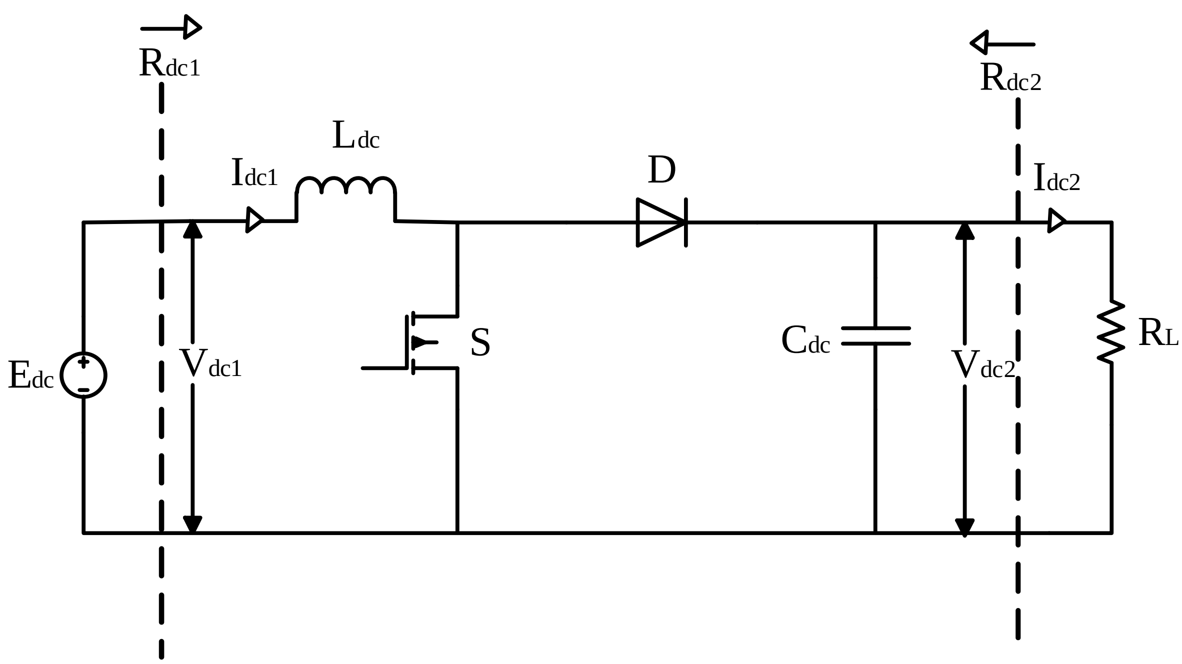

Figure 1.8. Boost chopper circuit

The AC output power from the generator is converted to DC power through diode rectifier and it is boosted by the boost chopper circuit [16] [17]. In this section, the operation of the boost chopper circuit is theoretically analyzed. The generator and the rectifier circuit is reduced into a DC power supply for ease of analysis. The inverter and grid together is modeled as a load resistance connected with DC link.

The circuit configuration of the boost chopper is shown in Fig 1.8. The energy is stored in L_{dc}, when S is on for the time t_{on} and, the energy is transferred to C_{dc}, when S is off for the time $toff$. Hence we get

$$V_{dc1}t_{on} = V_{dc2}t_{off} \ . \tag{1.8}$$

Rearranging the terms we get

$$V_{dc2} = \frac{t_{on}}{t_{off}}V_{dc2} \ \text{ and} \tag{1.9}$$

$$= \frac{1}{1-D}V_{dc1} \ , \tag{1.10}$$

where D, Duty ratio, is

$$D = \frac{t_{on}}{t_{on}+t_{off}} \ . \tag{1.11}$$

It is possible to assume that boost circuit and load resistance R_L, are reflected as a variable resistance varied by duty ratio from the viewpoint of the DC voltage source. This variable resistance R_{dc1} is defined as

$$I_{dc1} = \frac{V_{dc1}}{R_{dc1}} \ , \tag{1.12}$$

and similarly

$$I_{dc2} = \frac{V_{dc2}}{R_{dc2}} \ . \tag{1.13}$$

Assuming boost circuit is lossless , we get

$$V_{dc1}I_{dc1} = V_{dc2}I_{dc2} \tag{1.14}$$

and by substituting Eqn.(1.9) and Eqn.(1.10) in Eqn.(1.14), we get

$$I_{dc2} = (1 - D)(I_{dc1}) \ . \tag{1.15}$$

Dividing Eqn.(1.10) with Eqn.(1.15) we get

$$\frac{V_{dc2}}{I_{dc2}} = \frac{1}{(1 - D)^2} \frac{V_{dc2}}{I_{dc2}} \ , \tag{1.16}$$

which can also be written as

$$R_{dc1} = (1 - D)^2 R_L \ . \tag{1.17}$$

Hence from equation Eqn.(1.17) it can be inferred that the boost chopper from the viewpoint of the DC voltage source can be expressed as a function of the duty ratio.

1.7 Literature Review

This section provides a review of past and present strategies used in MPPT controllers that can be used for extracting maximum power from the available wind power. This section also summarizes various techniques that was previously used to build a Wind Turbine test bench system that can emulate the real time wind turbine characteristics.

1.7.1 Maximum Power Point tracking

The maximum power extraction algorithms researched so far can be classified into two main control methods, namely tip speed ratio (TSR) control and hill-climb search (HCS) control [18] [19]. TSR control method, proposed in [20], uses a wind speed estimation based system in order to track the peak power points. The wind speed is estimated using neural networks and using the estimated wind speed and optimal TSR, the optimal rotor speed command is computed as shown in Fig 1.9. Several variants of Hill climbing search methods have been developed so far [18] [21]. Authors of [19] proposed a principle that can search-remember-reuse. This method undergoes an offline training process and uses a memory for storing peak power points which are used later for tracking maximum power points.

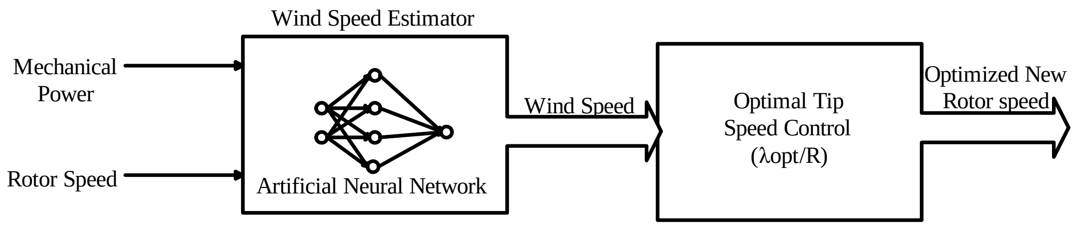

Figure 1.9. TSR control of MPPT

The performance of this algorithm improves over a period of time. This algorithm repeats itself until an accurate memory of turbine characteristics is established. The direct current demand control (DC-DC) utilizes the optimized relationship between the V_{dc} and I_{dm} recorded by the intelligent memory, and generates the command I_{dm} based on the present value of V_{dc} as shown in Fig 1.10 [19].

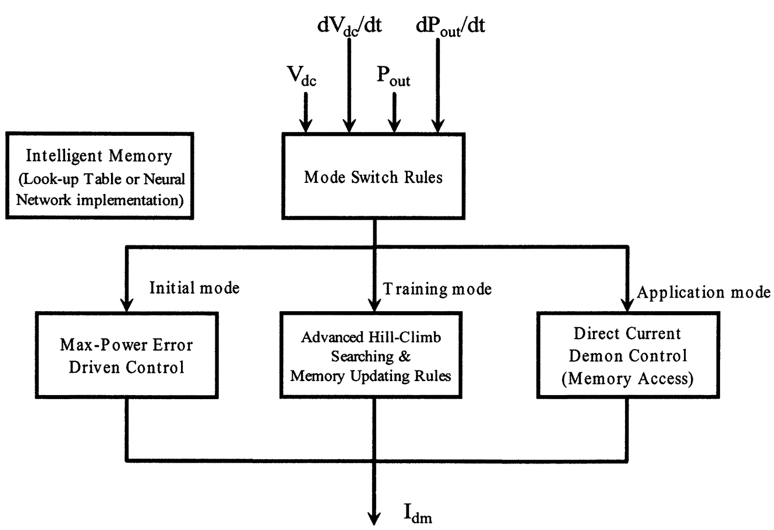

Figure 1.10. HCS control of MPPT

The MPPT control proposed in [22] is based on directly adjusting the duty ratio of the dc/dc converter by comparing successive generator output power measurements. The method is based on the fact that at the maximum power point $\frac{dP}{dw} = 0$. The dc/dc converter duty-cycle adjusts according to the control law of Eqn.(1.18) which ensures convergence to the maximum power point under any wind-speed condition as given by

$$D_k = D_{k-1} + C_1 \frac{\Delta P_{k-1}}{\Delta D_{k-1}} \; . \tag{1.18}$$

A HCS control method based on limit cycle is proposed in [23]. The MPPT control is performed via an integrator ramping up or down the current command signal of the grid side converter using the error in the dc link voltage regulated by a boost chopper as shown in Fig 1.11.

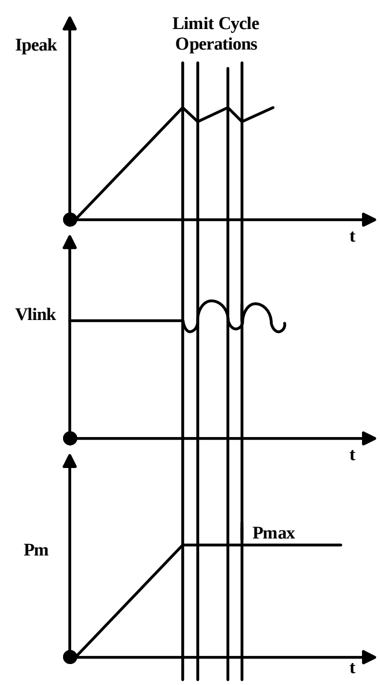

Figure 1.11. Operating principle of limit cycle

The reference current increases till the maximum power is obtained however, if it is increased further then the dc link voltage cannot be kept at constant because the power equilibrium cannot be maintained. Therefore, the dc link voltage begins to decrease and if it goes below a certain limit then, the integrator gain is changed to negative value decreasing the value of reference current.

Disturbance injection based HCS is proposed in [24]. The control algorithm injects a sinusoidal perturbation signal to the chopper. Then, the system output power is sampled at $\frac{\pi}{2}$ and $\frac{3\pi}{2}$ of each cycle, the difference of which decides about the next perturbation. The method does not require wind speed or rotor speed sensing. The HCS MPPT control method in [25] uses power as the input and torque as the controller output. The optimum torque output of the controller is applied to the torque control loop of a Direct Torque Controller(DTC) controlled PMSG. In the HCS method proposed in [26], the speed of the generator is indirectly controlled by controlling the output power as well as adjusting the electrical torque and hence obtains the the optimum speed for driving the power to the maximum point. The maximum power error driven mechanism, operates like a traditional hill-climbing method, drives the output power gradually increasing to its maximum value by regulating the direction of current command according to the power variation trend. The maximum power differential speed control produces an additional step of current command based on the instantaneous difference of generator speeds, so that it can prevent the wind turbine from stalling at the suddenly dropping wind speed and achieve the object of maximum power extraction.

A variable tracking step is used to track the maximum power point in [21]. The constant step size used in conventional controllers is replaced with a scaled measure of the slope of power with respect to the perturbed generator speed $\frac{\Delta P}{\Delta \omega}$. The variable step uses a larger step size when the operating point is far away from the peak due to the larger magnitude of $P - \omega$ slope and as the peak gets closer, the step size automatically approaches to zero. The method uses torque current and speed to compute power. The speed step is computed as

$$\Delta\omega = k.\frac{dP}{d\omega} \tag{1.19}$$

and the speed reference for the machine side converter control system is computed as

$$\omega^*(k+1) = \omega(k) + \Delta\omega(k) \ . \tag{1.20}$$

1.7.2 Wind Turbine Test Bench System

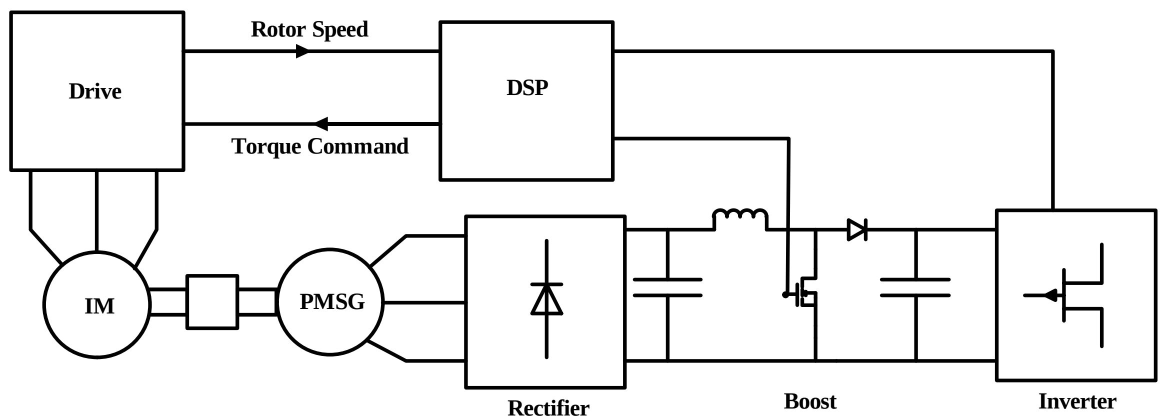

Figure 1.12. A Wind turbine Test Bench System

Due to the uncontrollable natural characteristics of wind speed and the large size of wind turbine [27], it is very difficult to perform experimental study in the laboratory [28]. A great deal of research has been focused on the development of wind turbine design in order to reduce the cost of wind power and to make wind turbine more economical and efficient. Research in wind energy conversion system involves high performance wind turbine simulators for the development of control system. To enhance the power quality of wind energy conversion system the wind turbine simulator is used as a necessary tool in research laboratories. The wind energy conversion system simulates the steady state wind turbine behaviors in a controlled environment without dependence on natural wind resource and actual wind turbines [29]. In the past few years, there has been extensive research to develop the wind turbine simulators which mainly focus on the aerodynamic model of wind turbine rotors [30].

Different types of machines have been used to emulate the turbine shaft. Both induction and DC motors have been used in wind turbine simulators [31] [32]. [31] presented a wind turbine simulator using the electromagnetic (EM) torque equation of a dc machine. The armature and field circuit was controlled so that the dc machine generates static characteristics of a constant pitch wind turbine. The wind turbine simulator as shown in the Fig 1.12 [32], aims to reproduce the mechanical behavior of wind turbine rotor, drive train and a gear box under dynamic and static conditions. The reference for the torque developed by the wind turbine includes the gradient and tower shadow effects that result in pulsating torques. In [33] a microcomputer-controlled SCR-DC motor was used to supply the shaft torque.

However these simulators are unattractive due to the use of large sized DC motors, which require frequent maintenance and are more expensive. The real wind system simulator with control strategies having output torque using induction motor was presented to give torque-speed curve of actual wind turbine. The wind turbine model and controller were developed on a C-language platform [29]. The emulator of wind turbine generator using dual inverter controlled squirrel-cage induction motor, which consist of two inverters, one as a prime mover and other as a variable speed generator was presented based on DSP processing [34]. The virtual model for prediction of wind turbine parameters was presented [35]. The wide range of wind speed with variable induction generator to enhance the power industry is expected to dominate the wind energy conversion systems.

1.8 Organization of thesis

Chapter 1 provides an introduction about Wind Energy Conversion Systems (WECS). The characteristics of the wind turbine and the principles governing the model are described in detail. It also elaborates on the components of the WECS like the DC-DC boost converter. The basic idea behind maximum power point extraction and a general concept of the proposed controller has also been presented. A literature review of existing Maximum Power Point (MPP) methods along with the design of Wind Turbine Test Bench Systems (WTTBS) is also presented

Chapter 2 gives an overview of the present wind turbine technology and several configurations available for wind power generation. The advantages and disadvantages of different types of wind turbines and wind energy systems has been discussed in detail. An outlay of various variants of WTTBS has been presented and its merits are analyzed.

Chapter 3 discusses few disadvantages in the conventional MPPT techniques. The operational principle of the proposed MPP tracking control algorithm has been explained in detail and analyzed with mathematical expressions. The advantages of the proposed controller over the conventional controller has been assessed. The simulation results from PSCAD/EMTDC are presented and is compared with the conventional hill climbing method.

Chapter 4 explains the MATLAB Simulink model of the proposed WTTBS used to emulate the wind energy system. Simulation results of the proposed WTTBS are presented and is compared with the real WECS. Factors effecting 3P oscillations has also been discussed in detail.

Chapter 5 discusses the actual hardware implementation. The advantages of using a DSP micro controller for control of a power conditioning system are discussed. It also provides specifications of the power conditioning unit used for experimental tests. Experimental results of the proposed WTTBS for various wind conditions under the same test are shown.

Chapter 6 summarizes the results from the thesis. This chapter also includes the original contributions of this research and suggestions for future work.

Chapter 2 Wind Energy Conversion Systems

Wind Energy Conversion System (WECS) consists of a turbine, generator, drive-train and control systems as shown in Fig 2.1. Wind turbines are primarily classified into two types. Vertical axis type and Horizontal axis type. Most of the recent wind turbines use three blade horizontal axis configuration.

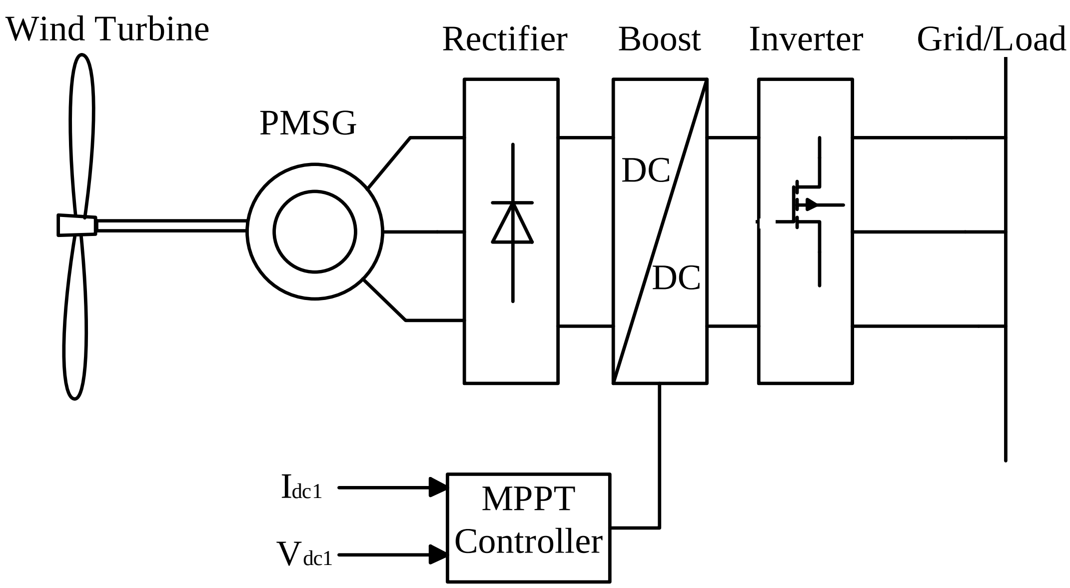

Figure 2.1. Wind Energy Conversion System

2.1 Horizontal axis Configuration

Horizontal axis wind turbine dominate the wind industry. Horizontal axis wind turbines as shown in Fig 2.2(a) [6], have the rotating axis horizontal or parallel to the ground. The advantage of this kind of wind turbine is that it is able to produce more electricity from a given amount of wind compared to other counterparts. It also has a high wind energy conversion efficiency, self-starting capability and access to stronger winds due to its elevation from the tower. The disadvantage of horizontal axis however is that it is generally heavier and it does not perform well under turbulent wind conditions.

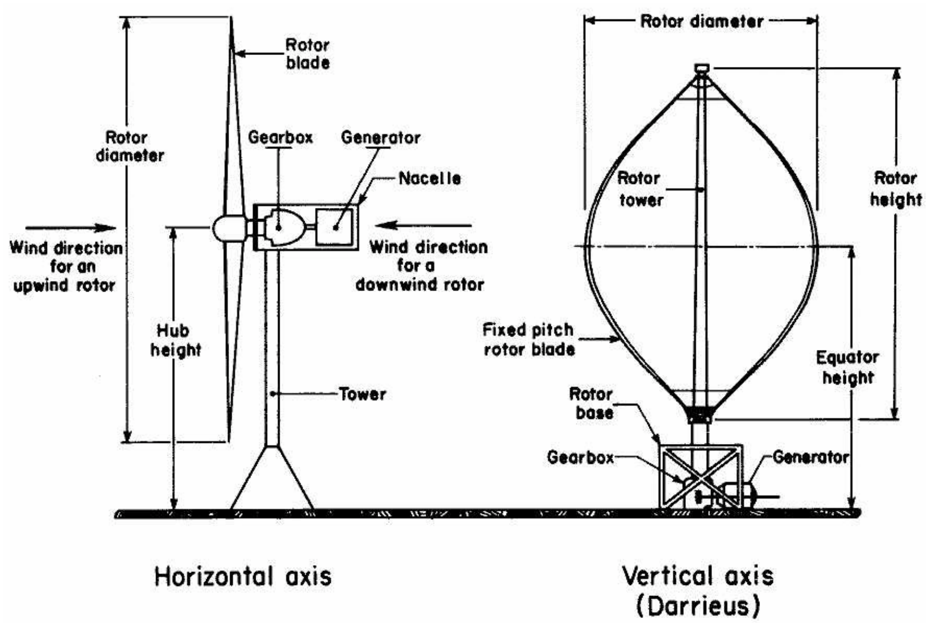

Figure 2.2. (a) Horizontal axis wind turbine (b) Vertical axis wind turbine

2.2 Vertical axis configuration

With vertical axis wind turbines the rotational axis of the turbine stands vertical or perpendicular to the ground as shown in Fig 2.2(b). Vertical axis turbines are primarily used in small wind projects and residential applications. These kinds of turbines have the ability to produce well in tumultuous wind conditions. Vertical axis turbines are powered by wind coming from all 360 degrees, and even some turbines are powered when the wind blows from top to bottom. Because of this versatility, vertical axis wind turbines are thought to be ideal for installations where wind conditions are not consistent. However, one major drawback of the vertical wind turbine is that it has low wind energy conversion efficiency and there are limited options for speed regulation in high winds. Its efficiency is around half of the efficiency of horizontal axis wind turbines. Vertical axis turbines also have high torque fluctuation with each revolution, and are not self-starting [6]. Hence keeping all these factors in mind, all the wind turbines considered in this thesis are Horizontal axis wind turbines.

2.3 Types of Wind Energy Conversion Systems

There are two main types of WECS, the fixed speed WECS and variable-speed WECS. The rotor speed of a fixed-speed WECS is fixed to a particular speed. The other type is the variable-speed WECS where the rotor is allowed to rotate freely. The variable-speed WECS uses power maximization techniques and algorithms to extract as much power as possible from the wind.

2.3.1 Fixed speed wind turbines

In a typical constant speed wind turbine, a gearbox is necessary between the low speed wind turbine rotor and high speed induction generator. Normally, an asynchronous generators are used in fixed speed WECS because of its inherent insensitivity to changes in torque [36] . A SCR controlled starter between the generator and the grid reduces the inrush current during the grid synchronization as shown in Fig 2.3. Consequentially, the system is characterized by stiff power train dynamics that only allow small variations in the rotor speed around the synchronous speed. Due to the mechanical characteristics of the induction generator and its insensitivity to changes in torque, the rotor speed is fixed at a particular speed dictated by the grid frequency, regardless of the wind speed. Since fixed speed systems do not allow significant variations in rotor speed, these systems are incapable of achieving the various rotor speeds that result in the maximum C_p value under varying wind conditions.

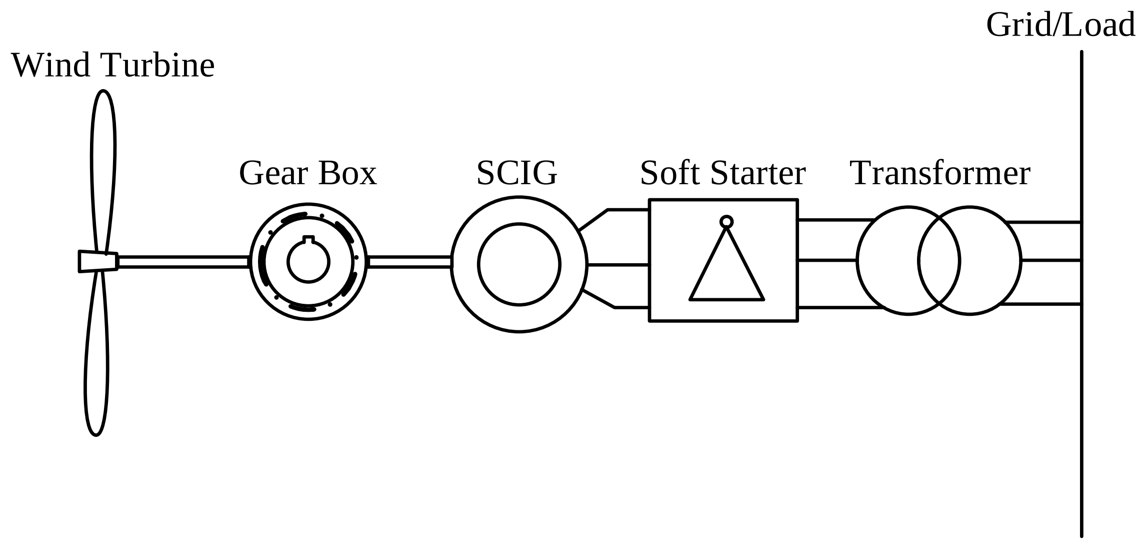

Figure 2.3. Constant Speed Wind Energy Conversion System

2.3.2 Variable speed wind turbines

A variable speed wind turbine can control the speed of the rotor and therefore operates at optimum tip speed thus offering more flexibility. So a variable speed wind turbine has the ability to produce more energy than its fixed speed counterpart. However such wind turbines require a power converter interface to synchronize its power to the main grid, thereby provide decoupling and control of the system. The mechanical stresses on the wind turbine are reduced since gusts of wind can be absorbed (i.e., energy is stored in the mechanical inertia of the turbine and thus reduces torque pulsations) [37]. Another advantage of this system is that the power quality can be improved by the reduction of power pulsations due to its elasticity. The disadvantages of the variable speed system include the additional cost of power converters and the complexity of the control algorithms. In this thesis, an optimum speed maximum power point tracking control algorithm is developed for variable speed wind energy systems to achieve maximum efficiency under fluctuating wind conditions.

2.4 Configurations of Variable speed WECS

Induction generators, Permanent magnet synchronous generator (PMSG) and wound field synchronous generator are widely used in high power turbines. However PMSG is preferred over other generators for small and medium power applications because of its high efficiency and power density. Normally the rotor speed has a very low RPM whereas the generator has a high RPM in the range of 1500-2000 RPM. So most of the variable speed wind turbines still need gearbox to normalize the rotor speed and generator speed. Direct drive configuration is a special type of configuration where a generator is coupled to the rotor of a wind turbine directly. Power converters are employed to convert and control the variable frequency and voltage to fixed grid levels.

2.4.1 Synchronous Generator

The stator of the generator is connected to the utility grid through power converters as shown in Fig 2.4. The main task of the stator side converter is to control the electromagnetic torque of the turbine. By adjusting the electromagnetic torque, the turbine can be forced to extract maximum power. The necessary magnetic field for operation of a synchronous generator is supplied by the DC current that flows through the rotor. A rectifier between the rotor and the utility converts the alternating current (AC) from the utility grid into direct current. Permanent magnet synchronous generators (PMSG) are common in low power, variable speed wind energy conversion systems. The advantages of using PMSG are its high efficiency and small size. However, the cost of the permanent magnet and the demagnetization of the permanent magnet material should be considered.

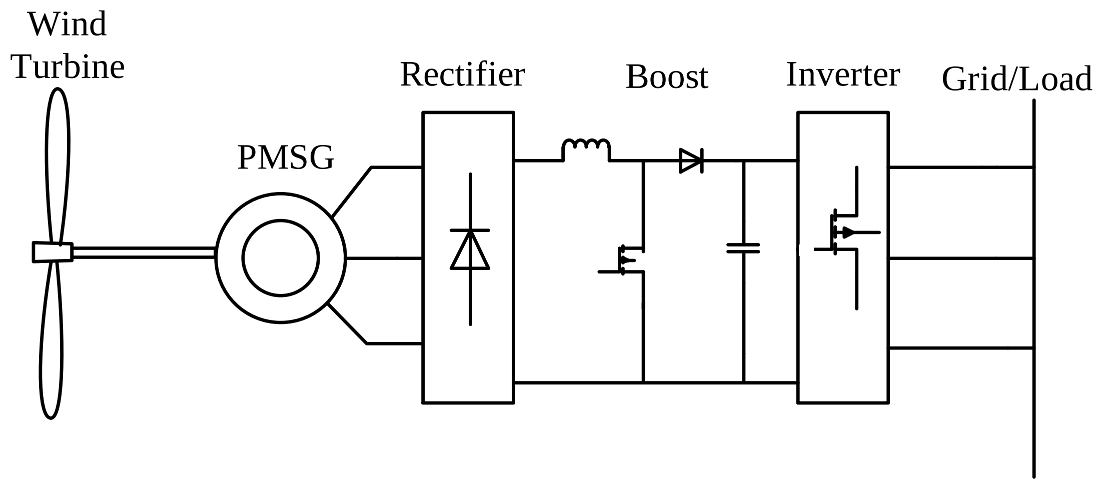

Figure 2.4. PMSG based Wind Energy Conversion System

In a PMSG, the stator windings are connected to the utility grid through a diode rectifier, boost converter, and a PWM inverter as shown in Fig 2.4. The diode rectifier rectifies the variable frequency and magnitude output AC voltages from the turbine.

2.4.2 Induction Generator

The stator is connected to the utility grid to provide the necessary magnetizing for machines operation. The rotor on the other hand is connected to the grid through power converters as shown in Fig 2.5. The rotor side converter regulates the electromagnetic torque and supplies some of the reactive power. To enable regulation of the electromagnetic torque, algorithms for extracting maximum power are implemented in the rotor side converter stage. The controller of the utility side converter regulates the voltage across the DC link for power transmission to the gird. There are reduced inverter costs associated with the Doubly Fed Induction Generator(DFIG) wind turbine because the power converters only need to control the slip power of the rotor. Another advantage of the DFIG is its two degrees of freedom; the power flow can be regulated between the two wind systems (rotor and stator) .

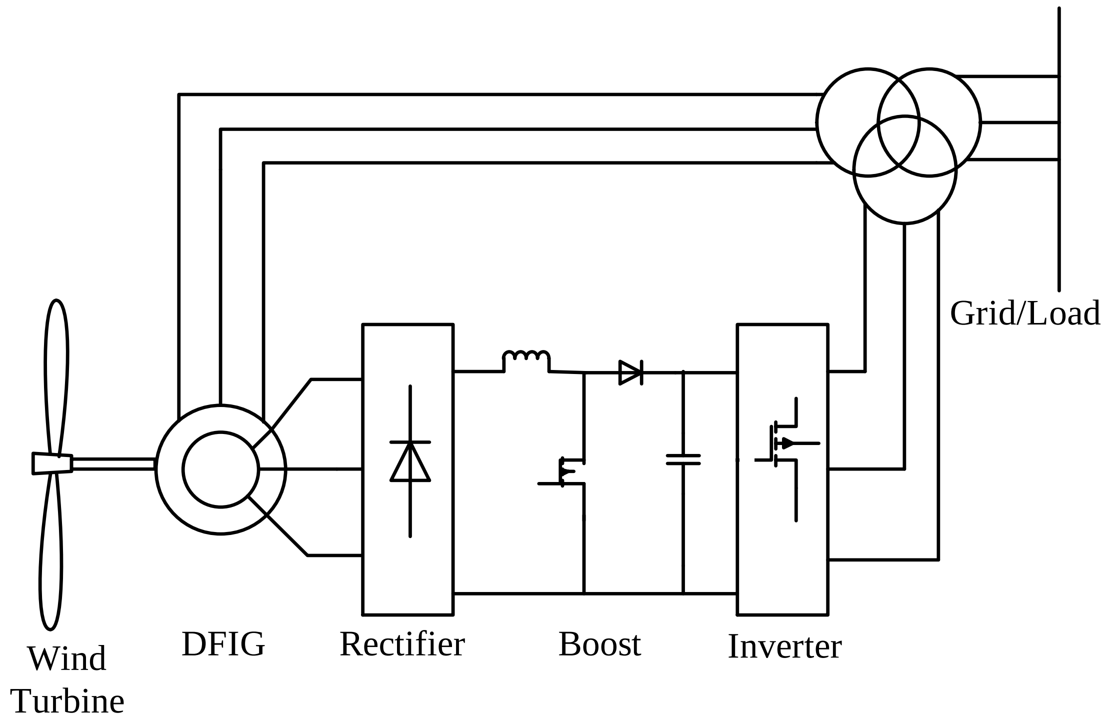

Figure 2.5. DFIG based Wind Energy Conversion System

This feature allows minimization of losses associated at a given operating point as well as other performance enhancements. A disadvantage of using the DFIG wind turbine, however, is that the generator uses slip rings. Since slip rings must be replaced periodically, and so the use of DFIG's translates to more frequent maintenance issues and long term costs than other brushless Motor

2.5 Wind Turbine Test Bench Systems

Design and development of WECS necessitates the need of detailed design processes to determine the best configuration, suitable location and a maximum power point tracking method, all of which requires numerous onsite experiments. Hence an accurate Wind Turbine Test Bench System (WTTBS), shown in Fig 2.6 is required to validate the design of laboratory concept prototypes. The WTTBS should be able to reproduce the characteristics of a real wind turbine for any given wind speed without depending on the natural wind. These systems can improve the effectiveness and efficiency of research in WECS. A WTTBS essentially consists of a torque controlled electrical motor and a controller. Several researches have been conducted in the past as shown in the literature [27]- [35].

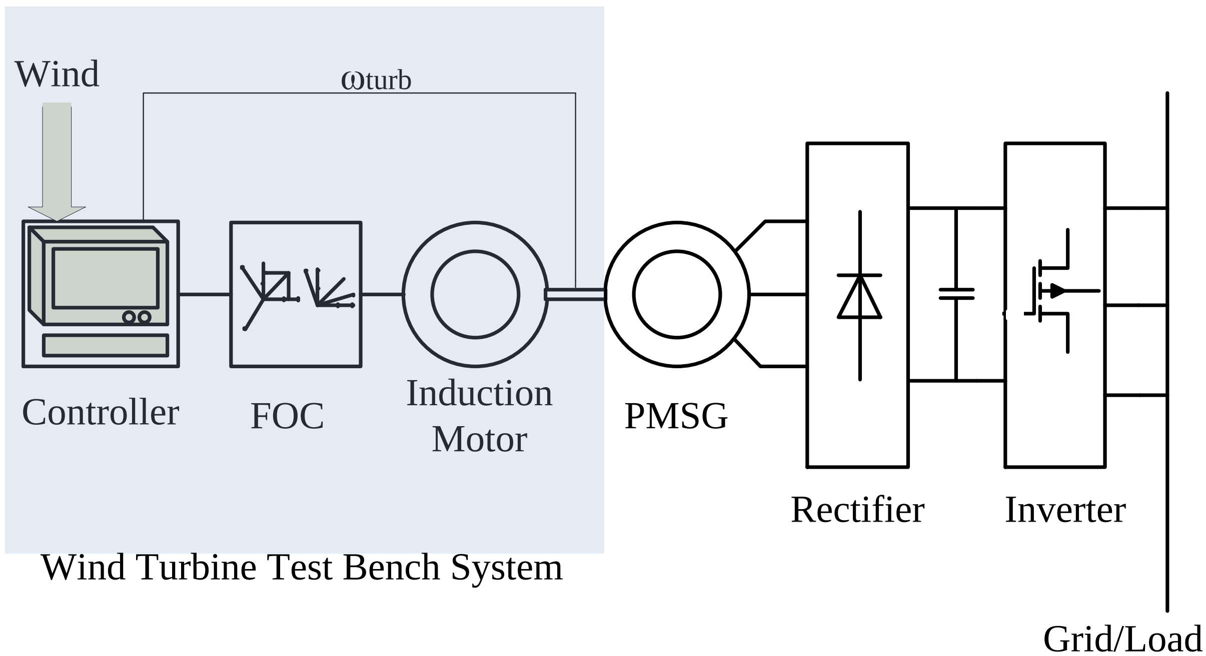

Figure 2.6. Wind Turbine Test Bench Systems

WTTBS can be classified into two groups based on the type of motor used.

2.5.1 DC Motor based WTTBS

WTTBS using DC motors often use armature and field voltage control methods to achieve static characteristics of a fixed pitch wind turbine. These simulators are simple, uncomplicated and usually do not consider the transient operations. DC motors was the most preferred selection to provide variable torque in the past due to its easily estimated and controlled torque. A thyristor rectifiers are usually used for driving a large dc motor yielding a simple and robust system. The reference for the armature current is calculated as a function of the wind speed and wind turbine speed to simulate the aerodynamic torque of a real wind turbine.

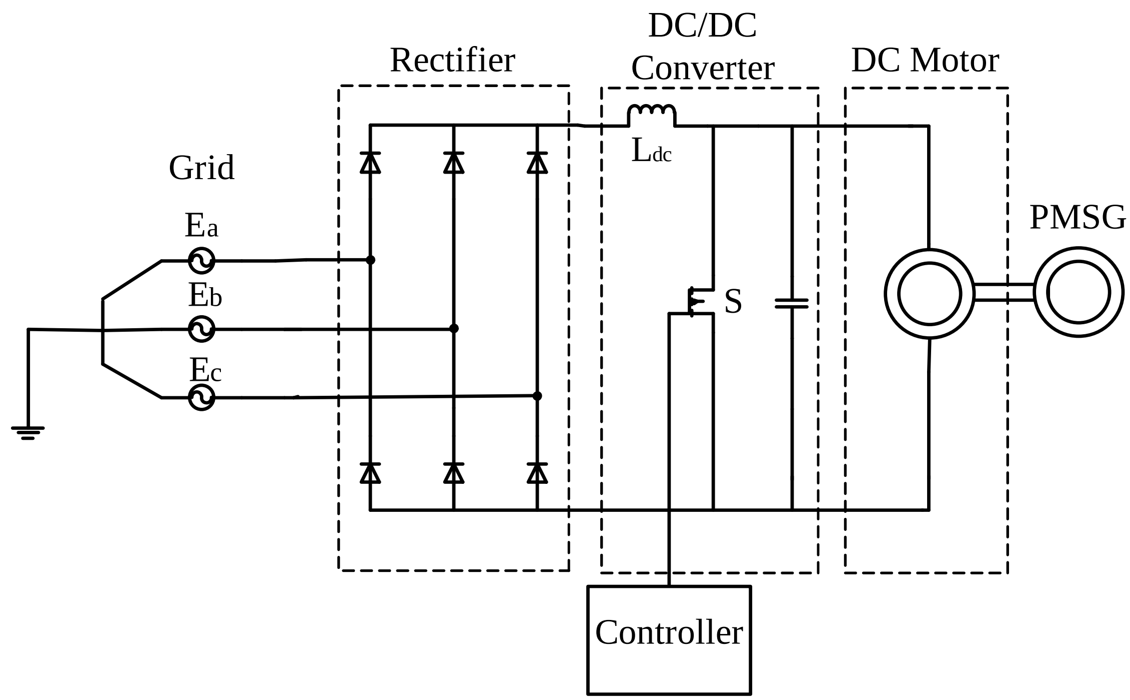

Figure 2.7. DC Motor Wind Turbine Test Bench Systems

The major disadvantage of this topology [38] is the induction of huge current ripple. The main ripple frequency introduced by a three-phase full converter is equal to six times the voltage source frequency (6th harmonic) that results in a 360 Hz current harmonic in the armature of the DC motor and in a unexpected ripple torque in the WTTBS. In order to get a better performance, few researchers developed a WTTBS with the thyristor rectifiers with a Buck - Boost converters supplied by a three phase diode rectifier as shown in Fig 2.7.

2.5.2 AC Motor based WTTBS

A dc machine, although is ideal from the standpoint of control is in general, bulky and expensive compared to an AC machine and it needs frequent maintenance due to its commutators and brushes. Hence an AC motor WTTBS as shown in Fig 2.8 is preferred [29]. Both synchronous and induction machine can be used in a WTTBS. The authors of [39] introduced an IGBT inverter controlled squirrel cage induction motor that is used to emulate the wind turbine. The induction motor parameters can be calculated by a control algorithm based on the model of the induction motor. The actual power and speed are detected by a torque-speed sensor mounted on the shaft of the induction motor instead of the traditional estimation methods to achieve the the power-speed curve of the wind turbine. Wind turbine simulator based on PMSM has some advantages such as high power density, small size, high precision and easy of control [40].

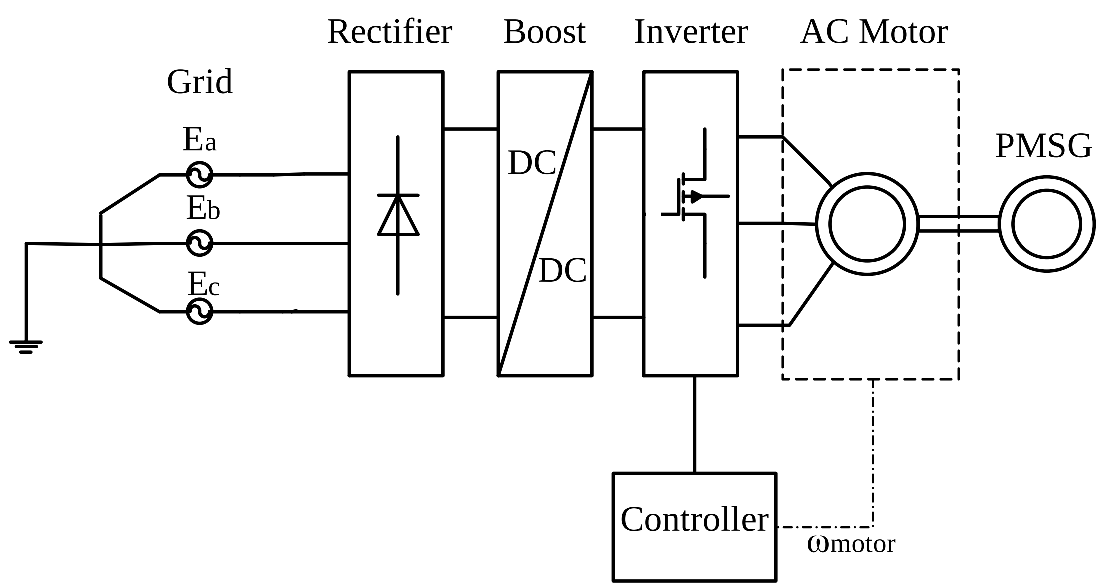

Figure 2.8. AC Motor Wind Turbine Test Bench Systems

Most of the earlier developed Wind turbine emulation system reproduce only the mechanical behavior of the fixed speed wind turbine. But in the real time scenario, the speed of the wind is never constant. It changes with time. Hence for an effective emulation, the test bench system has to reproduce the behavior of a turbine mechanical systems for dynamic conditions that includes variable wind speed input, wind sheer and tower shadow conditions.

The output torque is most commonly calculated by the use of aerodynamic equations. It is the function of variable wind speed, rotor speed and pitch angle. In order to simulate the dynamic process, the model of the mechanical system, especially the inertia of the turbine-generator should be simulated in real time.
Usually, the inertia of the simulated system and the real time turbine-generator system are different. In order to compensate for the difference, the torque of the generator which is mechanically coupled to the motor must be known. This compensation torque is added to the motor torque to obtain realtime torque . The torque together with simulated turbine torque is used to determine the acceleration of real wind turbine. However this method makes the simulator dependent on the generator side information which is not accessible.

Chapter 3 Proposed Algorithm

3.1 Introduction

The Existing HCS algorithm is most commonly used because of its ease of implementation. It is based on the following rule of thumb: if the operating power of the wind turbine is perturbed in a given direction and if the power drawn from the wind turbine increases, this means that the operating point has moved toward the MPP and, therefore, the operating power must be further perturbed in the same direction. Otherwise, if the power drawn from the wind turbine decreases, the operating point has moved away from the MPP and, therefore, the direction of the operating power perturbation must be reversed. However , A drawback of Hill Climbing MPPT technique is that, at steady state, the operating point oscillates around the MPP resulting in waste of some of the available energy [12] [41].

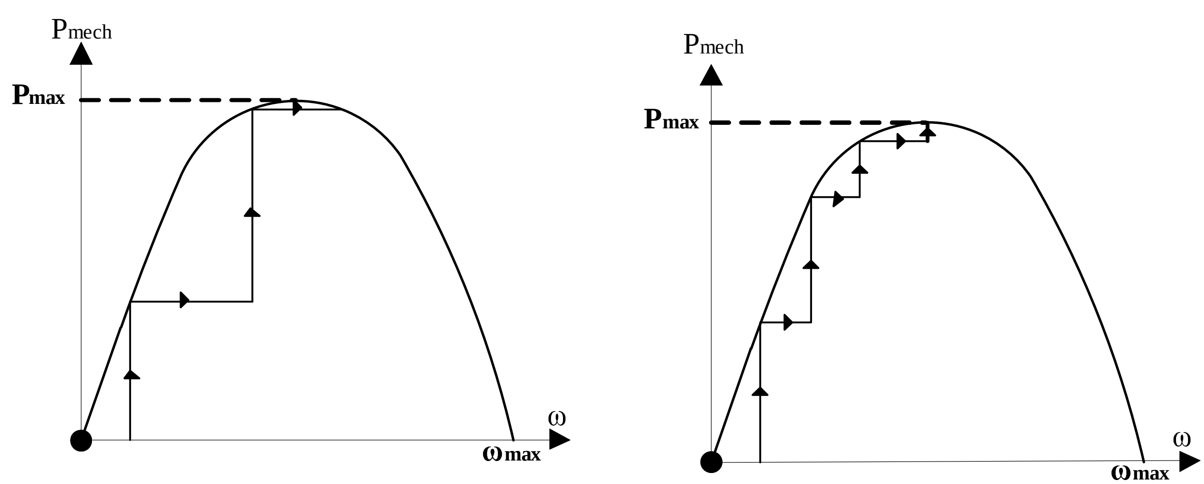

Figure 3.1. Conventional Hill climbing perturbation

This can be seen in Fig 3.1, a larger perturbation step size increases the speed of convergence but deteriorates the efficiency of the MPPT by amplifying the oscillations around the MPP P_{max}. This is because the HCS control does not at stop the process at MPP since it does not possess a peak detection capability, and hence, the oscillations are an unavoidable attribute of the HCS control [12]. A smaller step size boosts the efficiency, but then, the convergence speed becomes slower; therefore, the controller may become incapable of tracking MPP under rapidly varying wind conditions. Hence, in the conventional HCS control, a trade off always exists between the tracking speed and the control efficiency.

In the existing HCS algorithm, the direction of the next perturbation depends on the change in power due to the previous perturbation. Since the HCS algorithms treats the rest of the system as a black box , this rule can be overtly misleading , as the sign of the imminent perturbation might be caused by the wind change rather than the applied perturbation . This logic leads to failure in keeping track of MPP and HCS algorithm moves downhill.

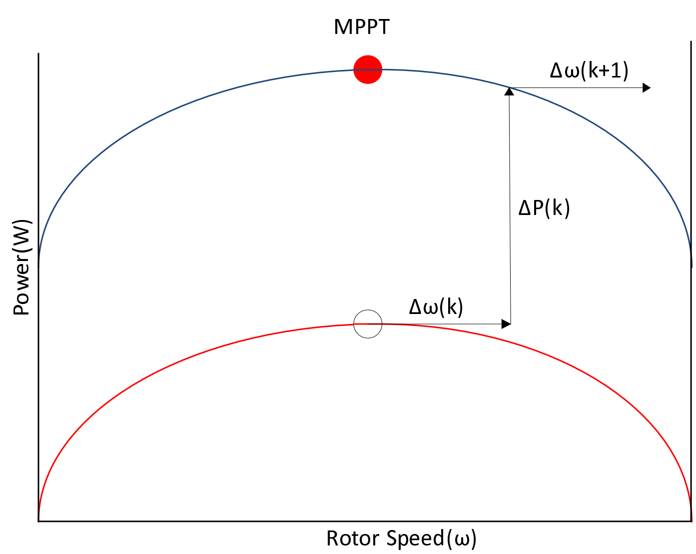

Figure 3.2. Logic failure in Conventional Hill climbing perturbation

3.2 Principle of the Proposed Algorithm

The novel MPPT algorithm proposed in this thesis uses the fact that a variable speed wind turbine's mechanical power P_m has a unique optimal power curve P_{opt} which exhibits a cubic function of the generator speed ω. Therefore, the optimal curve of a wind turbine's mechanical power is characterized by a unique constant k_{opt}, as given in

$$P_{opt} = k_{opt}\omega^3 \ . \tag{3.1}$$

By using Boost circuitry, as demonstrated in the previous chapter, we detect the maximum point successfully. Then k_{opt} can be simply extracted by measuring the corresponding power and rotational speed at the maximum power point. Once the peak is detected and k_{opt} is extracted, the latter can then serve as an accurate reference for the size and the direction of the next perturbation.

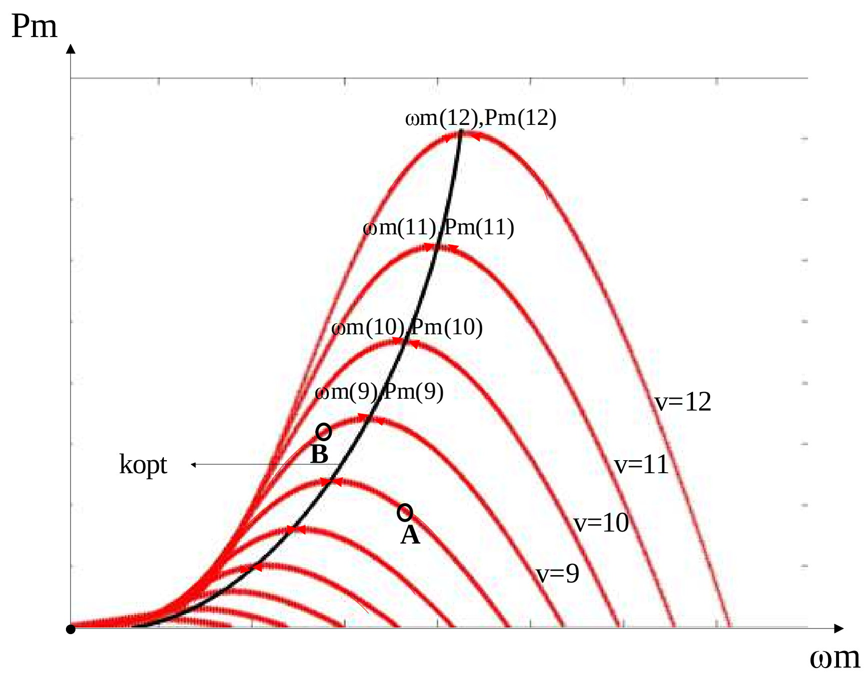

Figure 3.3. $P_m - \omega$ curves with its corresponding optimal curve k_{opt}

The optimal curve k_{opt} acts as a reference for the direction of perturbation. As demonstrated in Fig 3.3, an operating point "A" that lies on the right side of the curve tries to perturb in the direction of decreasing ω in order to converge to the optimal power point. The size of the perturbation can be dynamically changed by knowing the distance between the current operating point and optimal power point. This idea summarizes the intention of proposed algorithm. It provides us with a very effective solution to tackle the problems stated in the previous section. Now regardless of the wind change , the operating point lying anywhere, like A or B in Fig 3.3, will always move toward the optimal curve [12]. Also, it should be mentioned that the farther the operating point is from the optimal curve, the larger the perturbation size for faster tracking will be. However, as it converges into the optimal curve, the perturbation size will automatically approach zero, thus eliminating the speed efficiency compromise of HCS.

3.3 Methodology

Due to the rapidly varying wind conditions and generator load, optimal power characteristics , k_{opt} is never unique for a given wind turbine. Hence to account for the non uniqueness of k_{opt} , the algorithm has to be fine tuned to attain the absolute maximum power point. The proposed control incorporates a self tuning strategy by a novel process of scanning.

The flowchart in Fig 3.4 shows the Initialization process and two steps of operation. Initialization process searches for a k_{opt} with boost circuitry approach . Step 1 retains the system at the detected maximum, unless there is a change observed in wind velocity v . Step 1 gets into action under changing wind conditions and implements the novel Optimal Point search method via the earlier found k_{opt}.

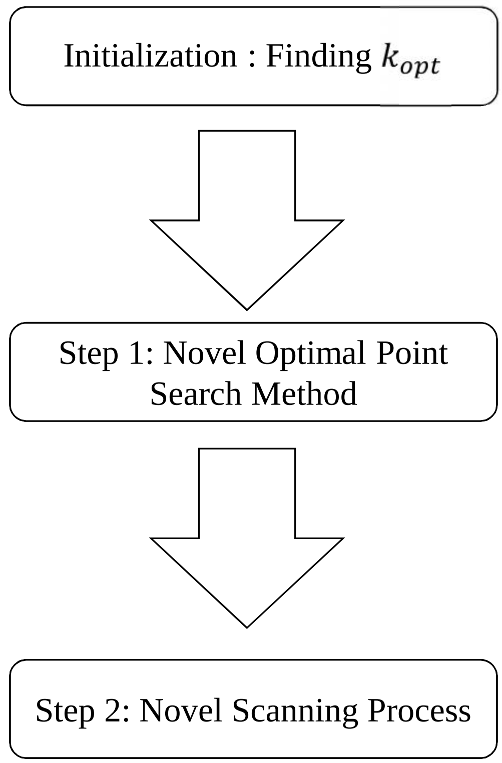

Figure 3.4. Flow of the algorithm under various constraints

Step 1 may not yield the true MPP, owing to the nonuniqueness of k_{opt} for different wind velocities, but still, it drives the operating point in the close vicinity of the true peak power. This control is very useful for fast tracking. It is to be noted that the control input is the duty ratio D of the converter which is generated by the MPPT controller. Step 2 implements the Scanning process, which fine tunes the obtained maxima. In the Scanning process the Duty ratio is made 1. Due to the effect of inertia, the current takes some time to reach its short circuit value. During this period , the controller continuously computes the active power and stops the further increase in current once the maximum power is reached.

3.4 Initialization: Determining k_{opt} by Optimum duty ratio algorithm using Boost Chopper

3.4.1 Introduction

Due to the nature of wind energy systems described in Chapter 1, the power available from the wind turbine is a function of both the wind speed and the rotor angular speed. The wind speed being uncontrollable, the only way to alter the operating point is to control the rotor speed. Rotor speed control can be achieved by using power electronics to control the loading of the generator. This MPPT process obtains the optimum duty ratio by theoretically differentiating the equation of the generated output power by duty ratio of the boost chopper. This optimum duty ratio yields the Maximum Power Point. k_{opt} is an approximate locus of all the maximum points in a wind turbine characteristic curve. From the past research on MPPT of wind turbines, it has been found out that k_{opt} curve is a linear third degree equation. Hence if we are able to locate one point in the locus, we can easily determine the equation of the locus. The maximum power point is defined by the power curve in Fig 3.1 where $\frac{\Delta P}{\Delta \omega} = 0$. Since the change in Duty ratio controls the speed of the rotor , the above expression can also be written as $\frac{\Delta P}{\Delta D} = 0$. Thus, the objective of this process is to find out an optimum duty ratio for which the condition of $\frac{\Delta P}{\Delta D} = 0$ is met [17].

3.4.2 Permanent Magnet Synchronous Generator

PMSG is preferred over other generators mainly due to its high efficiency. The EMF induced in PMSG is proportional to rotational speed . The equivalent circuit for one phase is shown in Fig 3. The constant of the generator is defined as k, and a field.

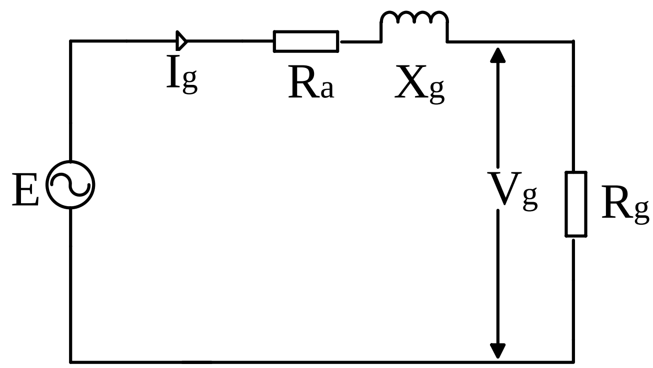

Figure 3.5. Equivalent circuit of PMSG per phase

Magnetic flux ϕ and mechanical angular velocity ω_g. The induced EMF is given by

$$E = k\phi\omega_g \ . \tag{3.2}$$

Terminal voltage V_g of the generator is

$$V_g = E - R_a I_g - jX_g Ig \ . \tag{3.3}$$

3.4.3 Design of Rectifier

The generator is connected to a rectifier circuit as shown Fig 3.6. It is assumed that the AC power generated from the generator is converted into DC power through diode bridge rectifier circuits

$$3V_g I_g = V_{dc1} I_{dc1} \ , \tag{3.4}$$

where, V_{dcl} and I_{dcl} are DC side voltage and current, respectively. The resistance in one phase of the rectifier circuits as viewed from the AC side is defined as R_g, and the maximum value of line-to-line voltage is defined as V_{LLPeak}. The mean value of DC voltage is

$$\begin{aligned} V_{dc1} &= \frac{3}{\pi} \int_{-\frac{\pi}{6}}^{\frac{\pi}{6}} V_{LLPeak} \cos\theta d\theta \\ &= \frac{3}{\pi} V_{LLPeak} \ . \end{aligned} \tag{3.5}$$

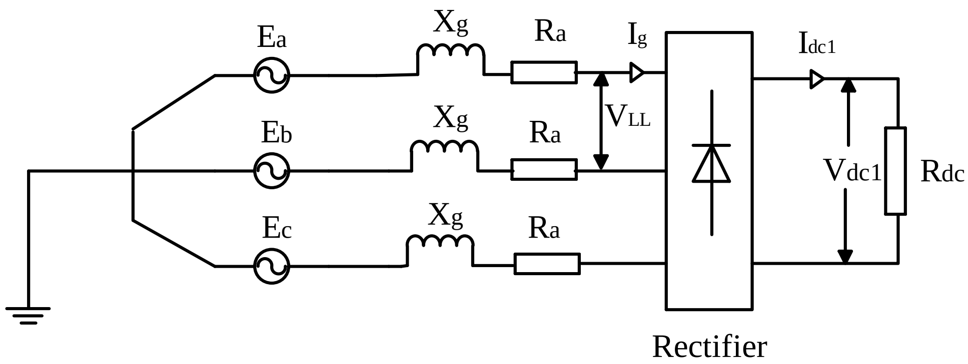

Figure 3.6. PMSG connected to a diode Rectifier

From these equations, the relationship between V_{dc1}, line to line voltage V_{LL} and phase voltage V_g is shown as

$$\begin{aligned} V_{dc1} &= \frac{3\sqrt{2}}{\pi} V_{LL} \\ &= \frac{3\sqrt{6}}{\pi} V_g \ . \end{aligned} \tag{3.6}$$

From Eqn.(3.4) and Eqn.(3.6), the equation of I_{dc1} and I_g are obtained as.

$$I_{dc1} = \frac{\pi}{\sqrt{6}} I_g \ . \tag{3.7}$$

3.4.4 Deriving the optimal duty ratio

From the boost circuit equations and rectifier equations as described in previous sections, it can be deduced that

$$R_g = \frac{\pi^2}{18}(1-D)^2 R_L \ . \tag{3.8}$$

The generator current of a PMSG from PMSG equivalent circuit can be given by

$$I_g = \frac{E}{(R_g + R_a) + jX_g} \tag{3.9}$$

the output power of the generator is given by

$$
\begin{aligned}
P &= 3V_g I_g cos\theta \\
&= 3R_g {I_g}^2 \\
&= \frac{\pi^2}{6}(1-D)^2 R_L \frac{(k\phi\omega_g)^2}{[\frac{\pi^2}{18}(1-D)^2 R_L + R_a]^2 + X_g^2} \ .
\end{aligned} \tag{3.10}
$$

The PMSG output power as shown in Eqn.(3.10) is dependent on generator speed ω_g and duty ratio D . Duty ratio of the boost chopper must be controlled in order to effectively extract the maximum power. There exist one duty ratio ,D_{max}, for which there exist a maximum power point. It can be computed as follows [17]

$$
\text{Let} \quad x = \frac{\pi^2}{18}(1-D)^2 R_L \ . \tag{3.11}
$$

Differentiating on both sides we get

$$
\frac{dx}{dD} = \frac{-\pi^2}{9}(1-D)R_L \ . \tag{3.12}
$$

Substituting the value of x in Eqn.(3.10) we get,

$$
P = \frac{3(k\phi\omega_g)^2 x}{(x+R_a)^2 + x_g^2} \ . \tag{3.13}
$$

For getting the optimal duty ratio we find the maxima of the curve by ,

$$
\begin{aligned}
\frac{dP}{dD} &= \frac{dP}{dx}\frac{dx}{dD} = 0 \\
&= (k\phi\omega_g)^2 (\frac{-\pi^2}{9})(1-D)R_L \\
&\frac{[R_a^2 + x_g^2 - x^2]}{(x+R_a)^2 + x_g^2)^2} = 0
\end{aligned} \tag{3.14}
$$

From the above equation D_{max} is derived as

$$
D_{max} = \frac{\pi\sqrt{R_L}}{\pi\sqrt{R_L} + 3\sqrt{2\sqrt{R_a^2 + x_g^2}}} \ . \tag{3.15}
$$

The variation of PMSG power with change in duty ratio is shown in Fig 3.7.

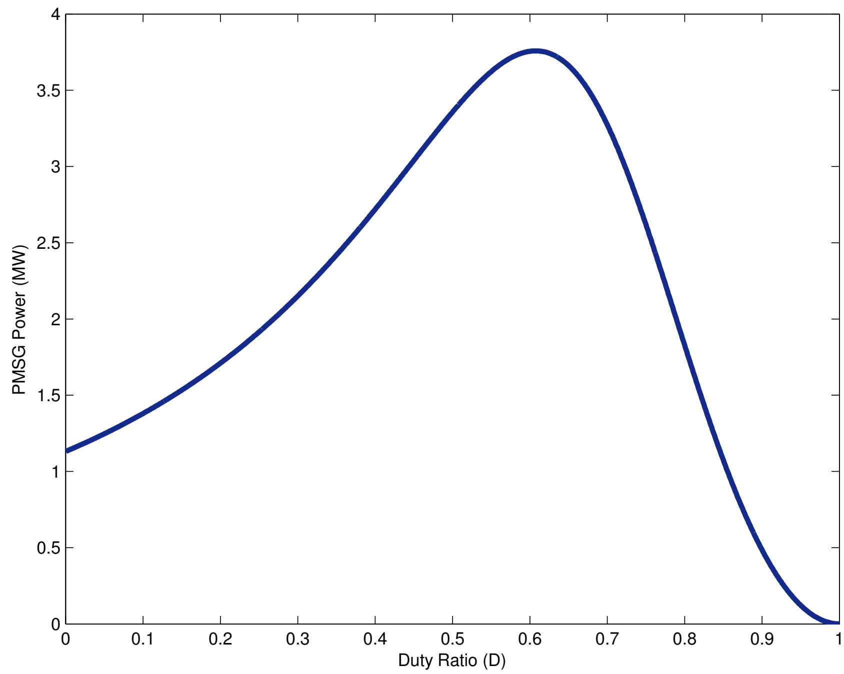

Figure 3.7. Rate of change of power with duty ratio

3.5 Step 1: Novel Optimal Point search method

The block diagram of the proposed WECS is illustrated in Fig 3.8. The uncontrolled rectifier, produces a dc voltage V_{dc1} proportional to the speed of the generator ω. The boost stage performs the MPPT control from the measured quantities of V_{dc1} and I_{dc1} from the rectification stage. Once the initial slope of the optimal curve is obtained, the operating point (ω_1, P_{in1}) of the WECS is coordinated with the maximum power point (ω_{opt}, P_{opt}) by regulating the boost converter (D) as described in the Eqn.(3.16). The proposed method is a two step adaptive approach control which adjusts the characteristic slope (k_{opt}) of the optimal cubic curve depending on the current operating conditions. Initially the k_{opt} of the turbine is obtained by Initialization process as described in the previous section. Once the initial slope of the optimal curve is obtained, the operating point (ω_1, P_{in1}) of the WECS is coordinated with the maximum power point (ω_{opt}, P_{opt}) by regulating the boost converter (D1) as

$$D(i+1) = 1 - \left[(1 - D(i)) \times \sqrt{\frac{V_{in}(i+1)}{V_{in}(i)}}\right] . \tag{3.16}$$

The desired turbine speed corresponding to the optimal slope k_{opt} and power $P_{in}(i)$, which is obtained from the product of $V_{dc1}(i)$ and $I_{dc1}(i)$, is represented by $\omega_g(i+1)$ and k_U is the rectification constant [42]. The relation between $\omega_g(i+1)$ and corresponding voltage $V_{dc1}(i+1)$ is as shown by

$$\omega_g(i+1) = \sqrt[3]{\frac{P_{in}(i)}{k_{opt}}} \text{ and} \tag{3.17}$$

$$V_{dc1}(i+1) = k_U \times \omega(i+1) . \tag{3.18}$$

The control algorithm runs in an iterative fashion by updating the duty cycle of the boost converter as shown in Eqn.(3.16). The operating point moves along the optimal power curve k_{opt} until the MPP (ω_{opt}, P_{opt}) for the current wind speed is reached. Once the MPP point is reached, the calculated reference voltage $V_{dc1}(i+1)$ would be same as previous iteration value $V_{dc}(i)$ and the duty cycle ceases to update as shown in Fig 3.9.

The duty cycle obtained in Eqn.(3.16) is dependent on the characteristic slope k_{opt} of the turbine. However the optimal curves are non unique for different wind speeds and also the generator-converter efficiencies are inconsistent. So, in order to adjust the k_{opt} corresponding to different wind speeds a novel scanning process is implemented.

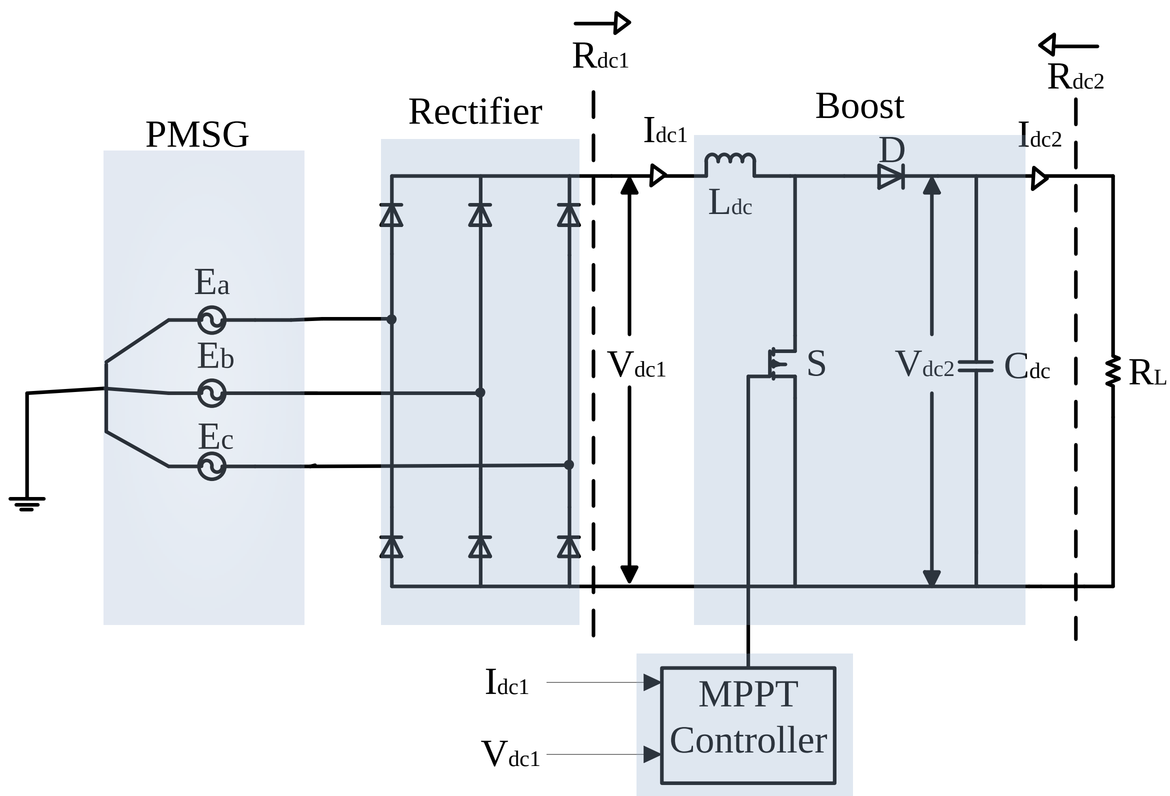

Figure 3.8. Proposed Power Conditioning systems for WECS

3.5.1 Calculation of Duty Ratio

The Initial value of the the duty cycle D1 is set arbitrarily within the limits of 0<D1<1, say 0.25. V_{in} and I_{in} are the voltage and current drawn by the rectifier and P_{in} is the numerical product of V_{in} and I_{in} as shown by Eqn.(3.19)

$$P_{in} = V_{in} \times I_{in} \; . \tag{3.19}$$

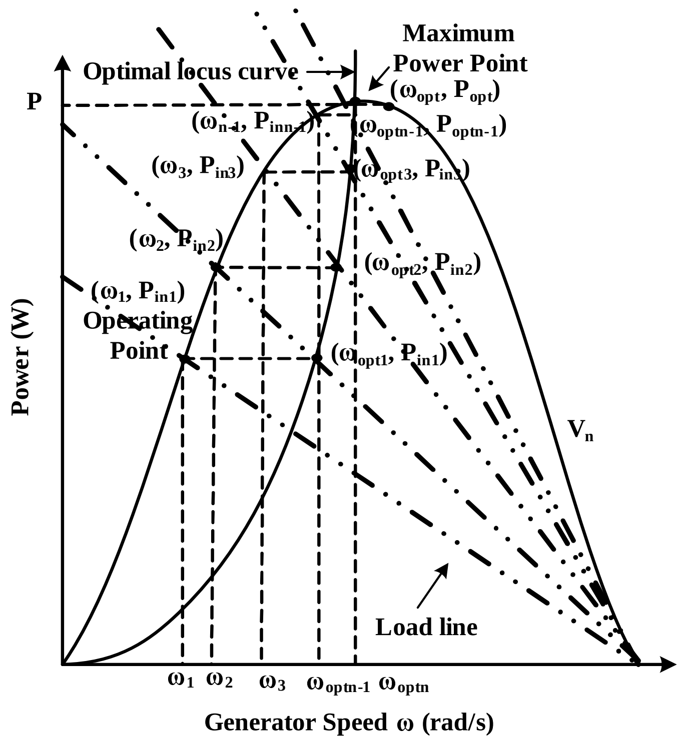

Figure 3.9. Load line following the optimum power curve

This P_{in} is made to follow the optimal power curve until it intersects with the turbine power characteristics. The duty cycle of the boost converter is calculated as follows: The duty cycle of the PWM to DC-DC boost converter can be expressed as

$$\frac{V_{dc}}{V_{in}} = \frac{1}{1-D} \quad \text{and} \tag{3.20}$$

$$\frac{I_{in}}{I_{dc}} = \frac{1}{1-D} \ . \tag{3.21}$$

Multiplying equation Eqn.(3.8) and Eqn.(3.9) we get,

$$\frac{V_{dc}}{V_{in}} \times \frac{I_{in}}{I_{dc}} = \frac{1}{(1-D)^2} \ . \tag{3.22}$$

Rearranging the equation , we get

$$D = 1 - \sqrt{\frac{V_{in} \times I_{dc}}{V_{dc} \times I_{in}}} \ . \tag{3.23}$$

In the discrete form , the duty cycle at the i^{th} iteration for the a iterative loop is given by

$$D(i) = 1 - \sqrt{\frac{V_{in}(i) \times I_{dc}(i)}{V_{dc}(i) \times I_{in}(i)}} \tag{3.24}$$

from Eqn.(3.19) we know that $P_{in}(i)$ is the operating power. The duty ratio is increased in such a way that the operating rotor speed $\omega(i+1)$ corresponds to operating power $P_{in}(i)$ and k_{opt} . This is given by Eqn.(3.6)

$$\omega(i+1) = \sqrt[3]{\frac{P_{in}}{k_{opt}}} \ . \tag{3.25}$$

However $\omega(i+1)$ is rewritten according to Eqn.(3.7)

$$V_{in}(i+1) = k_u \omega(i+1) \ . \tag{3.26}$$

The increased duty ratio $D(i+1)$ is calculated by

$$D(i+1) = 1 - \sqrt{\frac{V_{in}(i+1) \times I_{dc}(i)}{V_{dc}(i) \times I_{in}(i)}} \ . \tag{3.27}$$

By substituting Eqn.(3.13) in Eqn.(3.16) we get

$$1 - D(i+1) = \sqrt{\frac{V_{in}(i+1) \times (1 - D(i))}{V_{dc}(i)}} \ . \tag{3.28}$$

By the duty cycle $D(i+1)$ the slope of the load as seen by the turbine changes to the new operating point (ω_{opt1}, P_{in1}) corresponding to the $V_{in}(i+1)$. Now the operating point of the system will be (ω_{opt1}, P_{in1}) instead of (ω_{opt1}, P_{in1}) as that is just a virtual point measured and the operating point can only be on the $P - \omega$ curve. As the slope of the load line is adjusted with the help of the new duty cycle to be coinciding with rotor speed (ω_{opt1} the operating point will be the intersection of the load line with new slope and the $P - \omega$ curve. This process continues till the rotor speed ω_n coincides with the ω_{opt} of the optimum curve rotor speed as show in Fig 3.9. The duty ratio expressed in the mathematical form gives us

$$D(i+1) = 1 - \left[(1 - D(i)) \times \sqrt{\frac{V_{in}(i+1)}{V_{in}(i)}}\right] \ . \tag{3.29}$$

3.6 Step 2: A Novel Scanning Process

The scanning process is implemented by setting the duty cycle (D) to 1 after the operating point reaches the optimal point (ω_{opt}, P_{opt}). This results in a short circuit in the current path through the boost inductor L_{boost} and the switch S. Due to this, the voltage V_{in} tends to go to 0 and the current I_{in} starts to raise to its short circuit value. But this does not happen instantaneously owing to the presence of the inductor L_{boost} and the filter capacitor C_{in} which does not allow sudden change in current and voltage respectively as shown in Fig 3.10.

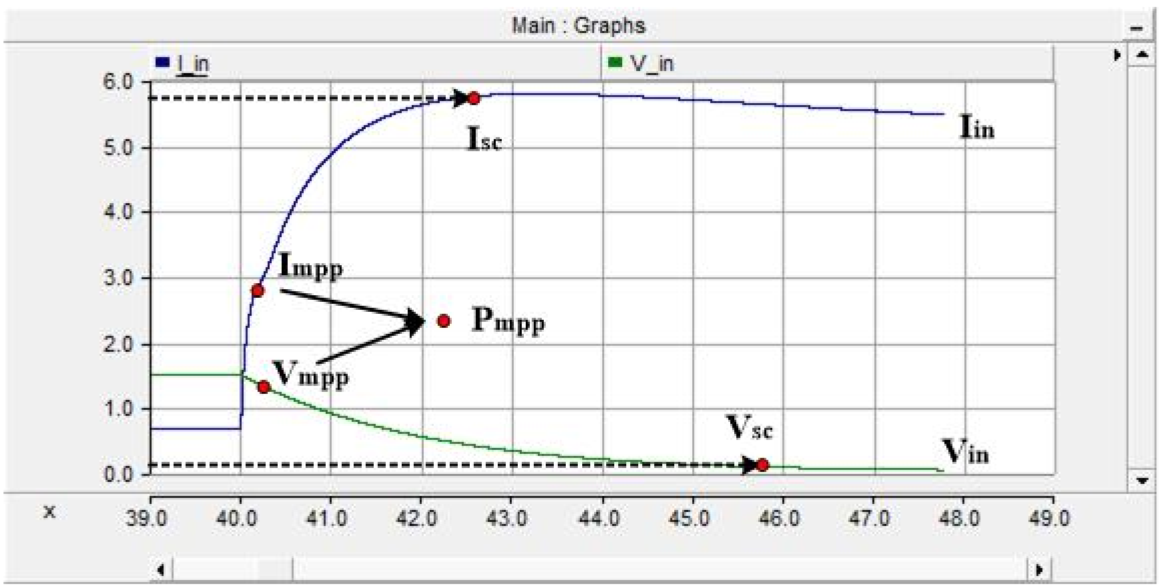

Figure 3.10. Rectification voltage and current during scanning process

This scanning process occurs for a very small duration of time (2 secs). During the scanning process, the controller continuously multiplies V_{dc1} and I_{dc1} and obtains the Power. This process is continued till the controller detects the change in power ($\Delta P < 0$).

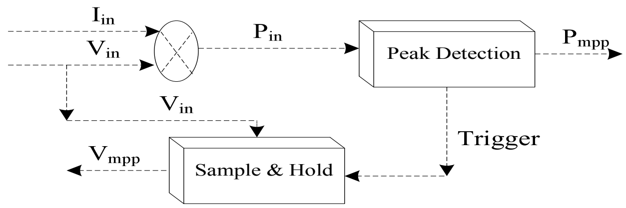

Figure 3.11. Block diagram representing Scanning process

Once the MPP is reached the boost output voltage is made to follow the V_{mpp} corresponding to the P_{mpp} corresponding to the duty ratio given by

$$D = 1 - \frac{V_{mpp}}{V_{dc2}} \ . \tag{3.30}$$

During this scanning process the maximum value of the power P_{mpp} and the corresponding voltage V_{mpp} are obtained as shown in Fig 3.10. Once the MPP is reached the characteristic slope k_{opt} of the turbine is updated as shown in Eqn.(3.18). The controller continuous to operate at the MPP until a change in wind speed or load current is detected.

Change in the duty ratio changes the load as seen by the turbine. Setting the duty ratio to 1, signifies that the PMSG is short circuited for a very small duration of time. During this transient time, the PMSG tries to deliver the maximum stable power for this transient time before it fall to zero. Hence this scanning controller tries to tap that maximum point to make the system very efficient.

3.7 Simulation Results

In order to validate the proposed controller, simulations were carried out for two scenarios . Scenario 1 implements the proposed novel controller method to track the MPP and Scenario 2 has the traditional Hill Climbing Method. The results of both the Scenarios are compared to prove that proposed controller is quick and effective in tracking the MPP. The results concerning the performance of the proposed method as shown in Fig 13.14-13.18. The performance of any MPPT method is tested with the change in windpseed.

3.7.1 Computation of Parameters

The proposed algorithm presented in the previous section is simulated in both MATLAB/SIMULINK and PSCAD and the operation of the algorithm has been verified. MATLAB computes the mathematical and logical parameters of the algorithm and communicates to PSCAD which is linked internally. PWM signals required to trigger the boost is simulated by mathematically multiplying the duty ratio and triangular wave block. The rectified voltage and current of PMSG is sensed and used by the MPPT algorithm to calculate the duty ratio.

(1) Simulated PMSG characteristics

Table 3.1. PMSG parameters

Parameter	Value
Number of Poles	100
Rated Speed	$\frac{2\pi f}{100} = 3.76$
Rated Power	2 MVA
Rated Voltage	0.69 kV
x_g	0.4 PU
Rated current	1450 A

(2) Computation of C_p at rated parameters

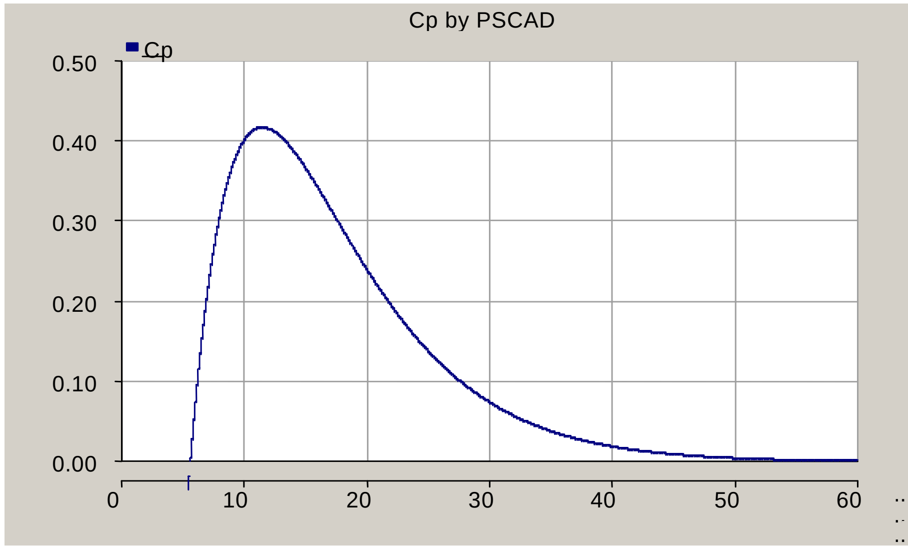

Figure 4: PSCAD Cp(γ)

Figure 3.12. C_p Characteristics with PSCAD approximation

PSCAD approximation of C_p is

$$C_p = 0.5(\gamma - 0.22\beta^2 - 5.6)e^{-0.17\gamma} \;, \tag{3.31}$$

where γ=2.237*(windspeed/PMSG speed) and β is the angle of incidence. The rated wind speed at which the PMSG produces rated power is 13 m/s Hence , from Table 3.1 we get

$$\gamma = windspeed \times \frac{2.237}{Hubspeed} \quad \text{and} \tag{3.32}$$

$$= 13 \times \frac{2.237}{3.1416} = 9.25 \;. \tag{3.33}$$

(3) Computation of Rated Power

In general the turbine rating is 20% more powerful than the generator because of the friction in the mechanical cycle:

Rated power of the generator: S_{gen}= 2 MVA

Rated Power of the Turbine : S_{turb}=1.2 * 2 = 2.4 MVA

(4) Computation of rotor radius and area:

$$P_{mech} = \frac{1}{2}\rho C_p(\lambda,\beta) A v_h^3 \text{ and} \tag{3.34}$$

$$= \frac{1}{2} \times 1.22 \times (0.4) \times A \times (13)^3 , \tag{3.35}$$

which gives : A=6716 m^2 and R=46.2 m.

3.7.2 Scenario 1: Proposed Controller

The proposed MPPT algorithm is tested for the 2.4 MW WECS rated at 13 m/s wind speed. The simulation is performed under varying wind conditions as shown in Fig 3.13.

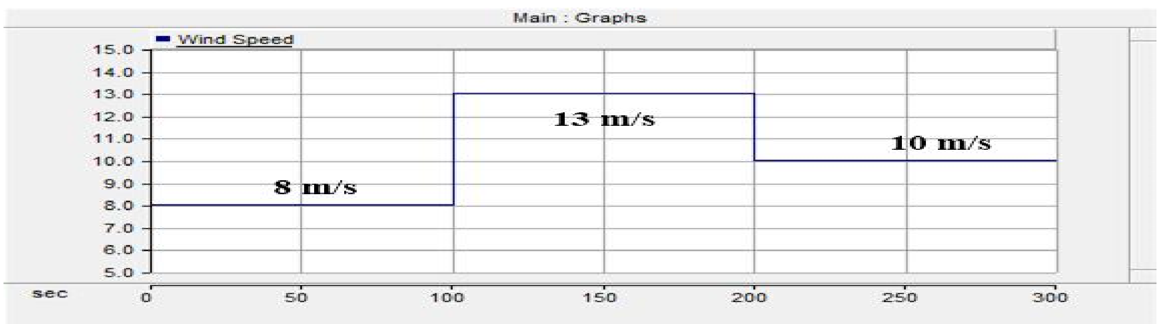

Figure 3.13. Simulated wind profile in (m/s)

The two step efficient process, proposed in this thesis, can be identified in the graph as shown in Fig 3.14. When there is a step change in the wind speed, the controller computes the Step 1 duty ratio by the novel Point search method at which the power attains its local maxima. The ramp up portion of the graph immediately after the step wind change depicts this process. The power keeps ramping up till the calculated duty ratio is reached where it attains the local maxima. Once the calculated duty ratio is attained, the controller begins its Step 2: Scanning process to fine tune the process. This scanning algorithm quickly scans the global maxima by making the duty ratio of the boost as one. The process comes to halt once the controller identifies the global maxima and continues to be in the same state until a next step change in wind speed occurs. Fig 3.15 and 3.16 clearly demonstrates the novel scanning process. The moment duty ratio is made one, the Voltage begins to droop and Current starts to increase to a point where the power reaches global maxima. Fig 3.17 shows the cyclic nature of the generator phase current and Fig 3.18 shows its corresponding variation in the Rotor speed.

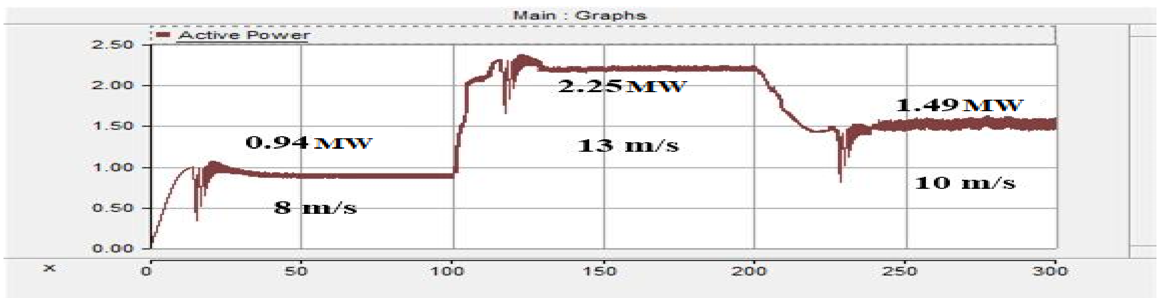

Figure 3.14. Power generated under MPPT control in (KW)

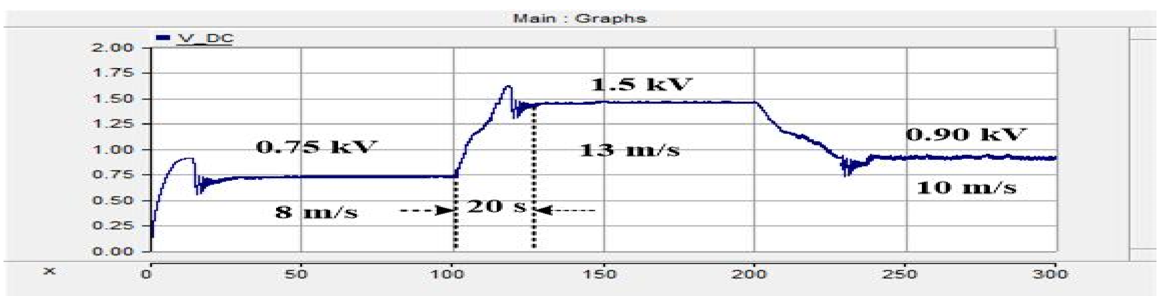

Figure 3.15. Rectified output voltage of the wind turbine in (kV)

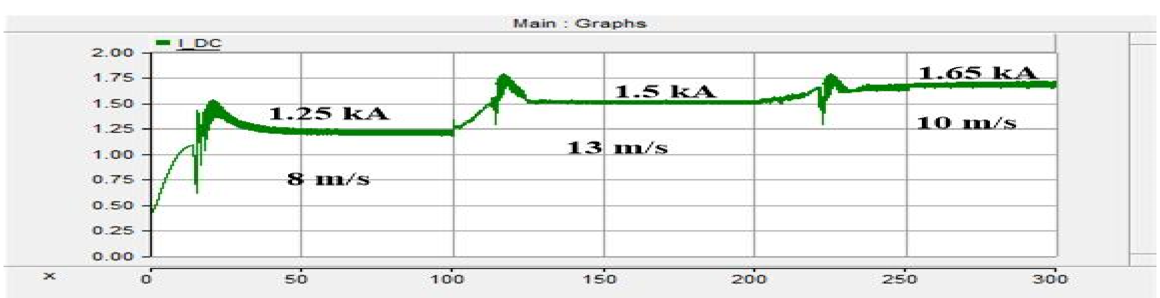

Figure 3.16. Rectified output current of the wind turbine in (kA)

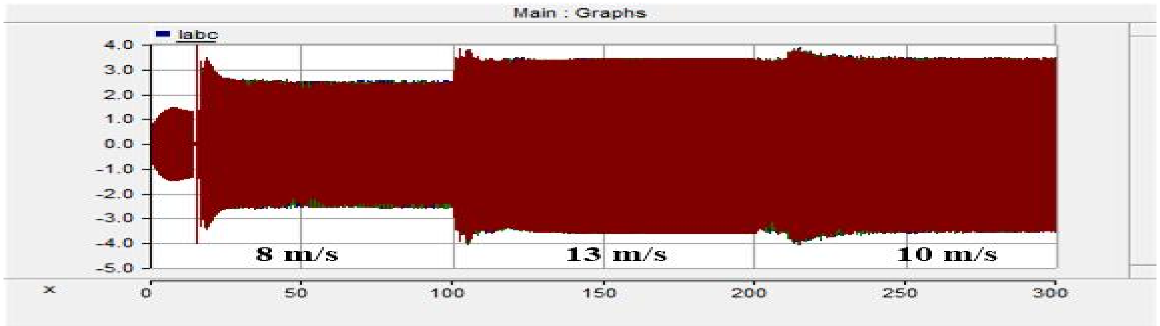

Figure 3.17. PMSG output current of the wind turbine in (kA)

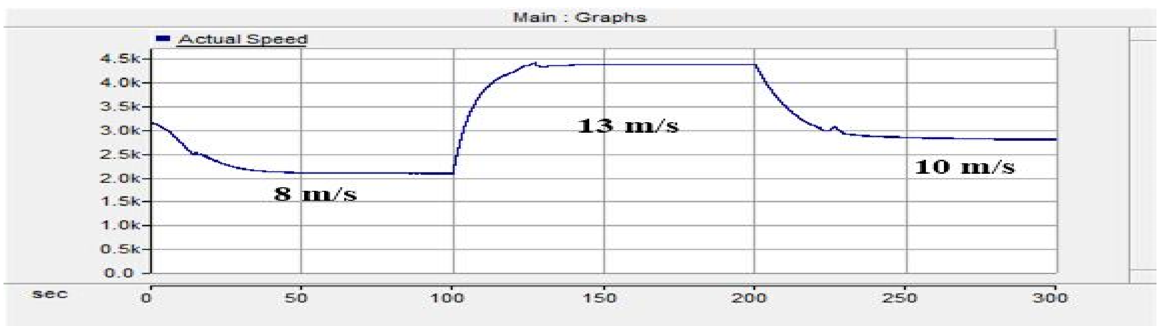

Figure 3.18. Power generated under MPPT control in (KW)

3.7.3 Scenario 2: Traditional Hill climbing

For the same wind profile, Fig 3.19-Fig 3.21 shows the implementation of MPPT with the traditional Hill climbing algorithm on the same 2.4 MW WECS system. It is to be noted that , during a step increase in windspeed from 8 to 13 m/s, the new algorithm exhibits a very steep slope as compared with the old one to instantly catch up with the added available energy. Proposed algorithm 20 seconds to track the MPP whereas the traditional HCS takes 60 seconds to reach the same MPP as shown in Fig 3.19. The output voltage and the rectified currents in the WECS using the traditional HCS also exhibits very sluggish characteristics .

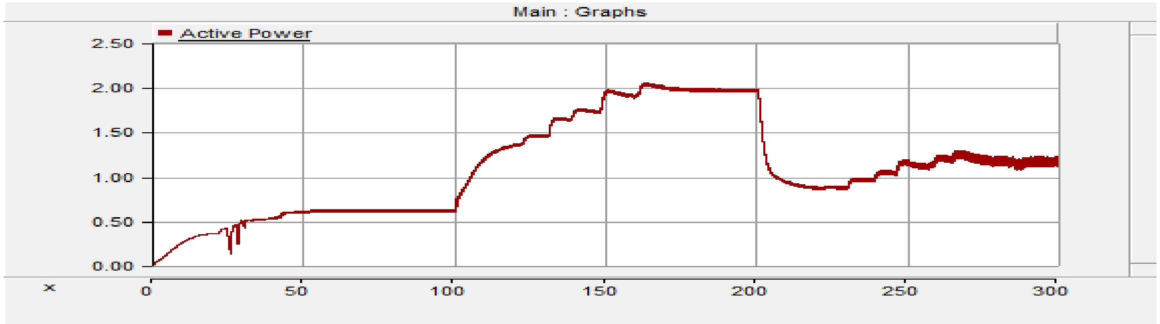

Figure 3.19. Power generated under MPPT control in (KW)

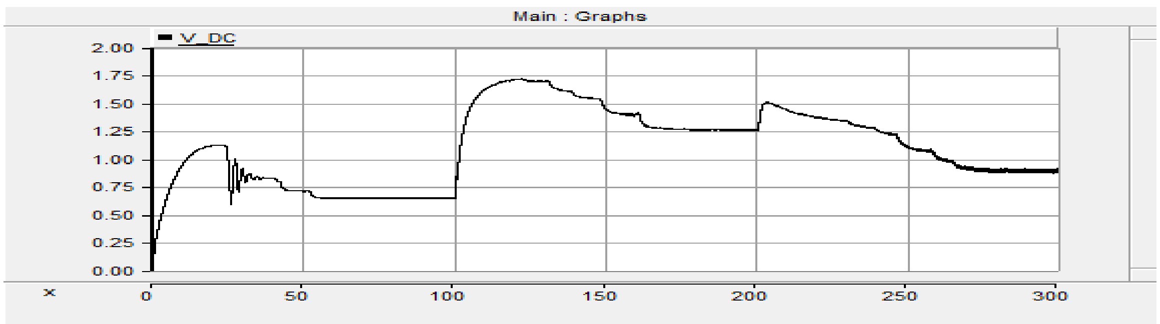

Figure 3.20. Rectified output voltage of the wind turbine in (kV)

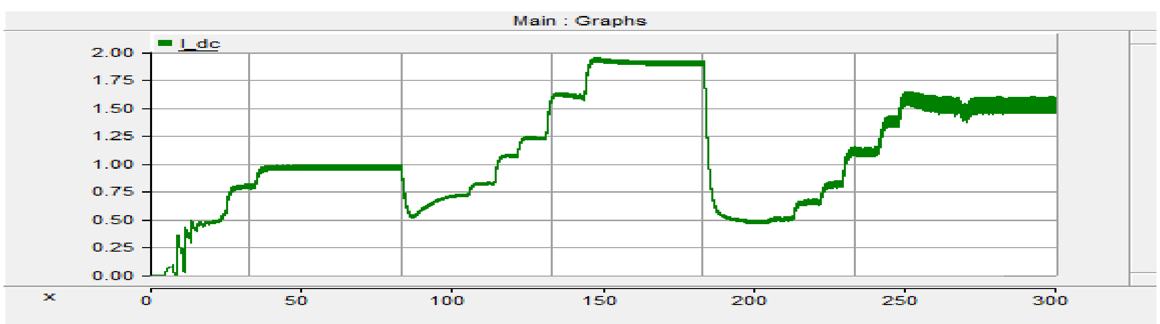

Figure 3.21. Rectified output current of the wind turbine in (kA)

Chapter 4 Modeling of Test Bench System

The objective of this chapter is to design a prototype of variable speed WECS simulator for a certain operational condition under variable wind speed. In this chapter variable speed induction motor drive using vector control is interfaced in WECS as an alternative to make the real time wind emulator for wind energy researchers as shown in Fig 4.1. The basic power curve from wind generator is implemented using a Digital Signal Processor and interface of induction motor through an inverter control system. The induction motor is operated in a wide speed range using Field oriented control scheme. The laboratory prototype consists of 1/4 HP, 415 Volts, 60Hz induction motor controlled by a voltage source inverter for various wind speed. The result verifies that the wind turbine simulator can reproduce the steady state characteristics of a given wind turbine at various wind conditions

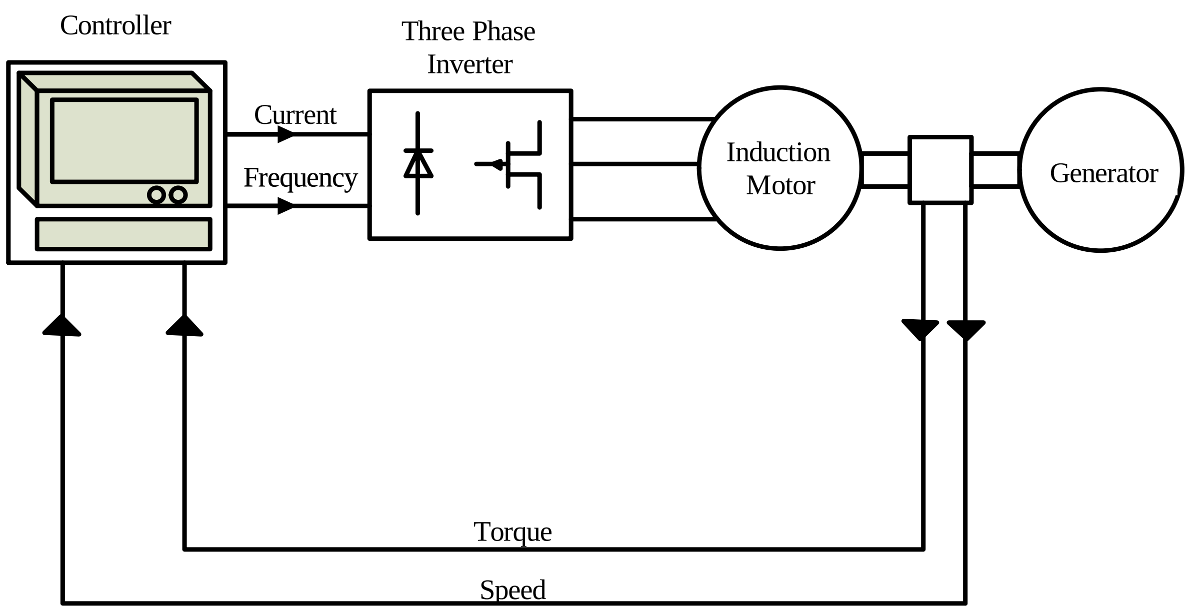

Figure 4.1. Structure of Wind Turbine Test Bench System

4.1 System Modelling

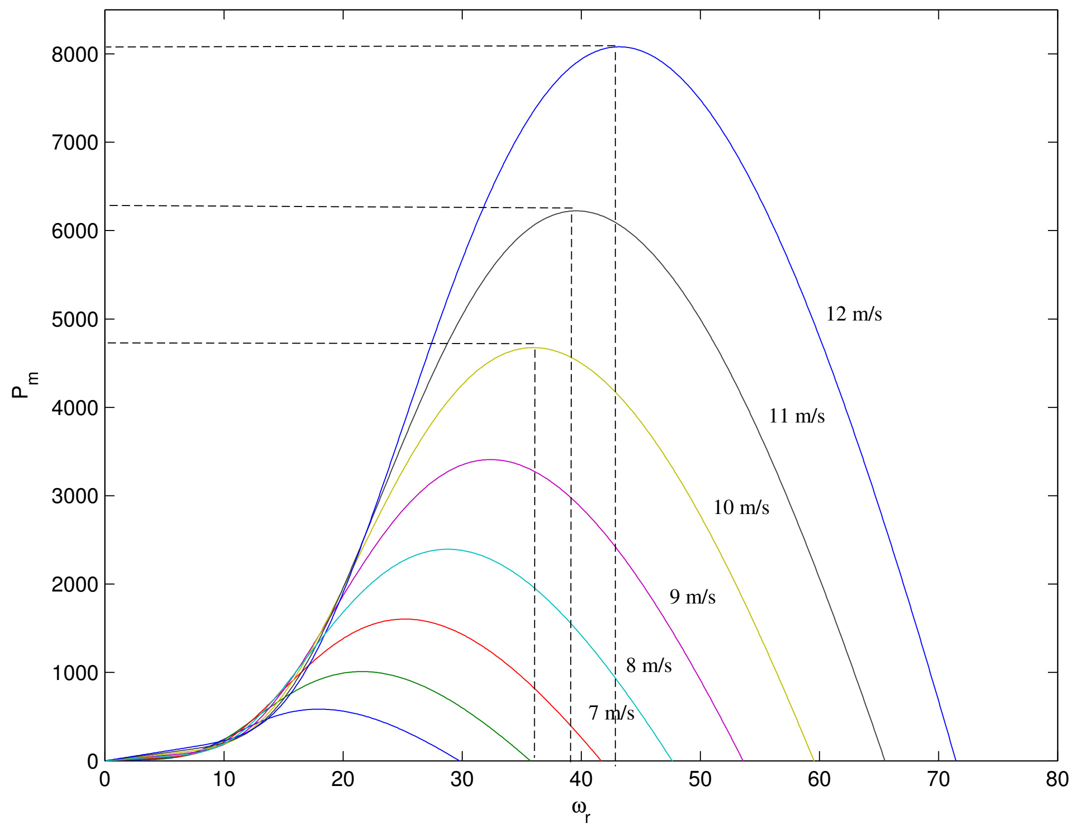

Figure 4.2. Power Chara of a WECS

The steady-state wind turbine model is given by the power speed characteristics shown in Fig 4.2. The curves in Fig 4.2 represent the characteristics of a 8-kW, three-blade horizontal axis wind turbine with a rotor diameter of 2.5 m. These curves can be obtained by wind turbine tests or calculated during the design by manufacturers. At a given wind speed, the operating point of the wind turbine is determined by the intersection between the turbine characteristic and the load characteristic. Usually, the turbine load is an electrical generator, such as an induction generator, synchronous generator, or permanent-magnet (PM) synchronous generator. From (4.1) it is noted that the shaft power of the wind turbine (P_m) is related to its shaft speed(n) and windspeed (v)

$$P_m = \frac{1}{2}\rho A c_p v^3 \ . \tag{4.1}$$

In a wind turbine test bench system, the power-speed characteristics of a wind turbine are physically implemented by an induction motor drive. The shaft power (P_m) and speed (n) of the induction motor represents the power and speed of the wind turbine rotor. An inverter fed IM is used to drive a load (i.e., a generator as if it were driven by a real wind turbine). In order to reproduce the turbine characteristics of Fig 4.2 in a laboratory, a DSP based control system is developed [29]. The wind speed signal needed for the test bench system is supplied from wind profiles which can be obtained from measured wind data of a site or can be set in any artificial form by users. Thus, researchers can conduct their studies on wind turbine drive trains in a controllable test environment in replacement of an uncontrollable field one.

4.2 Induction Motor Modeling

4.2.1 State Vector Model

The space vector equations for three phase induction machines in any arbitrary reference frame can be written as

$$d\bar{V}_s = r_s \bar{I}_s + \frac{d\bar{\psi}_s}{dt} + j\omega_k \bar{\psi}_s{}^k \ , \tag{4.2}$$

$$d\bar{V}_r = r_r \bar{I}_r + \frac{d\bar{\psi}_r}{dt} + j(\omega_k - \omega)\bar{\psi}_r{}^k \ , \tag{4.3}$$

$$d\bar{\psi}_s = L_s \bar{I}_s + M\bar{I}_r \ \text{ and} \tag{4.4}$$

$$d\bar{\psi}_r = L_r \bar{I}_r + M\bar{I}_s \ , \tag{4.5}$$

where ω_k and ω are the angular velocities of arbitrary reference frame and induction motor respectively.$\bar{V}_s$,$\bar{I}_s$,$\bar{\psi}_s$ are the space vectors for stator voltage, current and flux respectively. Similarly $\bar{V}_r$,$\bar{I}_r$,$\bar{\psi}_r$ are rotor voltage current and flux. The aim of vector control is usually to decouple the stator current into flux producing and torque producing components (i_{ds} and i_{qs}) respectively in order to obtain a decoupled control of flux and electromagnetic torque. For this vector control strategy the frame of reference is fixed to the rotor flux linkage vector, the q-component of this flux vector is zero.

$$\frac{d\psi_r}{dt} + \frac{\psi_{rd}}{\tau_r} = \frac{M}{\tau_r}.i_{sd} \text{ and} \tag{4.6}$$

$$T = \frac{3}{2}.\frac{P}{2}.\frac{M}{\psi_r}.(\psi_{rd}).i_{sd} \text{ .} \tag{4.7}$$

The rotor flux estimation is done by

$$\frac{d\psi_s}{dt} = V_s - r_s I_s \text{ and} \tag{4.8}$$

$$\psi_r = \frac{L_r}{M}(\psi_s - \sigma L_s I_s) \text{ ,} \tag{4.9}$$

where $\sigma = 1 - \frac{M^2}{L_s L_m}$.

Here flux estimator is assumed to be ideal.

4.2.2 Inertia Model

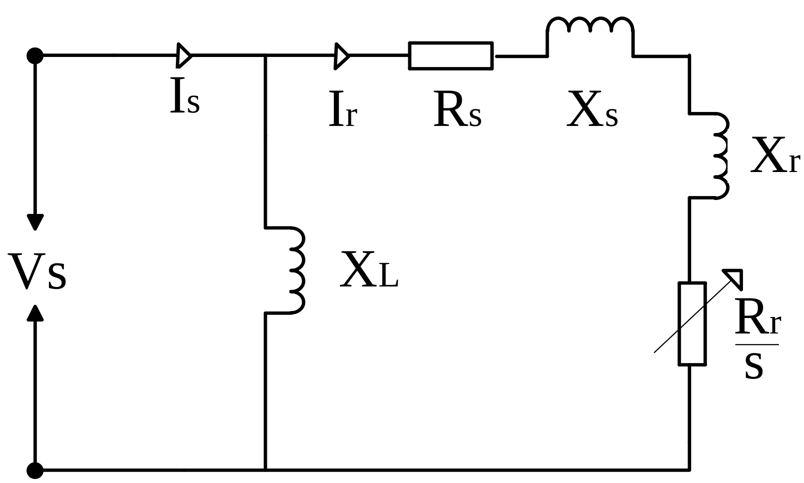

Figure 4.3. Equivalent circuit of an Induction motor

The model of an induction machine is highly nonlinear and mutually coupled [27] [29]. The complexity of the model is dictated by the purpose for which the model is employed. A simplified equivalent circuit model of an induction machine is shown in Fig 4.3 It is used to develop an appropriate controller with an approximate input-output model which relates the stator voltage input V_s , and the outputs, namely the angular speed ω_r and the developed torque T_m. The model is established based on the following assumptions.

- The dynamics of the subsystems are neglected as its time constant is smaller than the mechanical subsystem.
- Saturation and parameters are neglected.
- Core losses of the machines are neglected.
- The impedance of magnetizing circuit is considered larger than the stator impedance.

Table 4.1. Induction Motor parameters

Parameter	Value
R_s	50
L_s	47
3	31
4	35
5	45

The stator terminal voltage V_s is approximately considered as air-gap flux generated emf V_m. The rotor induced voltage V_r' causes rotor current I_r' at a slip frequency ω_{sl}, which is limited by rotor resistance and reactance. The phase diagram represents L_m, R_s are the magnetizing inductance and stator resistance and L_s, L_r are the stator and rotor inductance referred to input. The induction model consists of an algebraic equation which governs the flux linkage $\phi = \frac{V_s}{\omega_e}$ where ω_e is the supply frequency.

The magnitude of current I_r can be written as in

$$I_r = \frac{V_s}{\sqrt{(R_s + R_r/s)^2 + (\omega_e(L_s + L_r))^2}} \ . \tag{4.10}$$

The torque expression can be written as [27]

$$T_e = 3\frac{P}{2}{I_r}^2\frac{R_r}{s\omega_e} \ . \tag{4.11}$$

The laboratory test bench system comprising of induction motor drive has to produce the same inertia that a real wind turbine produces in the field. Hence a Compensation torque is added to the Induction motor torque to accurately emulate the effect of large turbine rotor inertia for a given wind speed. The actual blade torque can be represented by (4.12)

$$T_{turb} = (J_{turb} + J_g)\frac{d\omega_{turb}}{dt} + T_g \ . \tag{4.12}$$

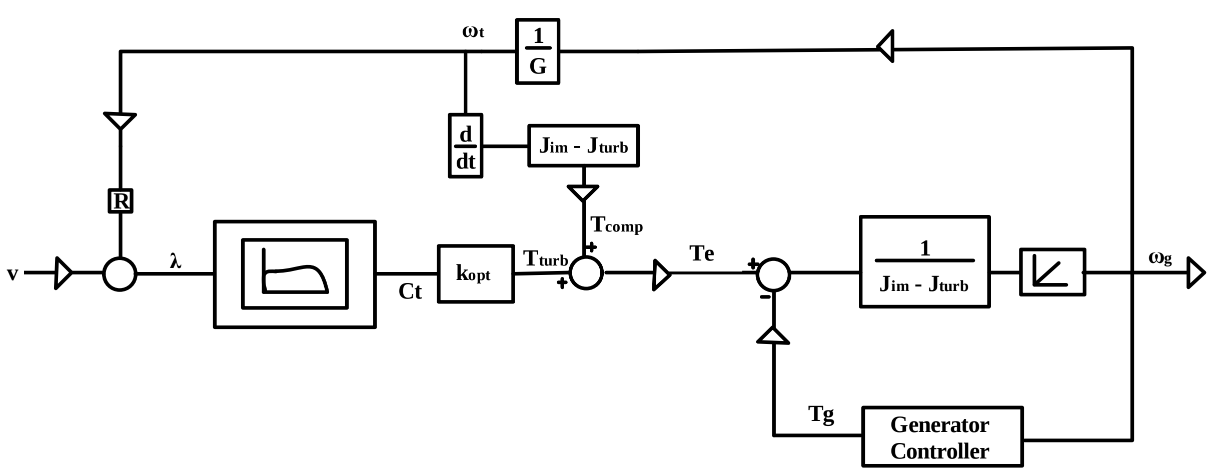

Figure 4.4. Inertia Calculation

An induction motor substitutes the blade of the wind turbine, where the motor torque TM can be represented by equation (3.5)

$$T_e = (J_{im} + J_g)\frac{d\omega}{dt} + T_g \ . \tag{4.13}$$

Assuming that the test bench system is gearless, that is dynamic characteristics of the wind turbine is same as that of blade , $d\omega_{turb} = d\omega$ ans

$$T_e = T_{turb} + (J_{im} - J_{turb})\frac{d\omega}{dt} \ , \tag{4.14}$$

where $T_{compensation} = (J_{im} - Jturb)\frac{d\omega}{dt}$ is the compensation torque.

4.3 Field Oriented Control

4.3.1 Introduction

This thesis is experimented on Texas Instruments Piccolo F2806xF Instaspin FOC platform. The technical details of the system is referred from the datasheet. A simple control such as the V/Hz strategy has limitations on the performance. To achieve better dynamic performance, a more complex control scheme needs to be applied, to control the induction motor. With the mathematical processing power offered by the microcontrollers, advanced control strategies are implemented, which use mathematical transformations in order to decouple the torque generation and the magnetization functions in an AC induction motor. Such de-coupled torque and magnetization control is commonly called rotor flux oriented control, or simply Field Oriented Control (FOC) as shown in Fig 4.6.

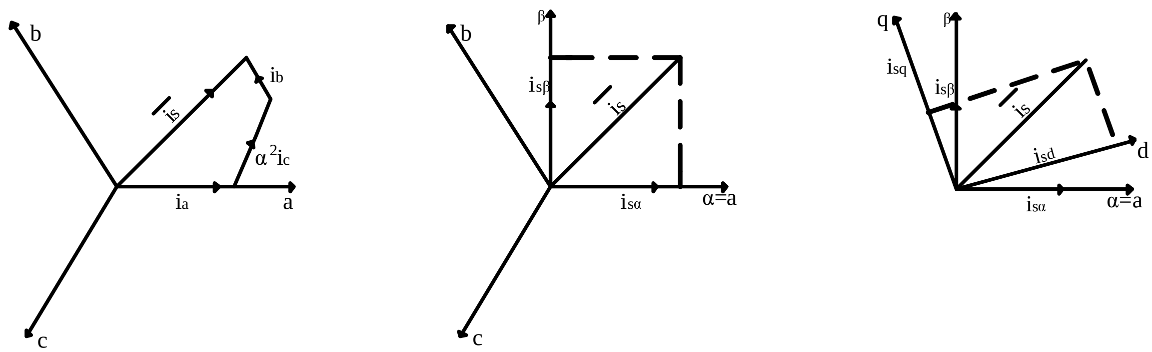

Figure 4.5. Field Oriented Control of induction motor

4.3.2 Control Techniques

To understand the Field Oriented Control technique, we first have an overview of the separately excited direct current (DC) Motor. In this type of motor, the excitation for the stator and rotor is independently controlled. An electrical study of the DC motor shows that the produced torque and the flux can be independently tuned. The strength of the field excitation (i.e., the magnitude of the field excitation current) sets the value of the flux. The current through the rotor windings determines how much torque is produced. The commutator on the rotor plays an interesting part in the torque production. The commutator is in contact with the brushes, and the mechanical construction is designed to switch into the circuit the windings that are mechanically aligned to produce the maximum torque. This arrangement then means that the torque production of the machine is fairly near optimal all the time. The key point here is that the windings are managed to keep the flux produced by the rotor windings orthogonal to the stator field. Induction machines do not have the same key features as the DC motor. However, in both cases we have only one source that can be controlled which is the stator currents.

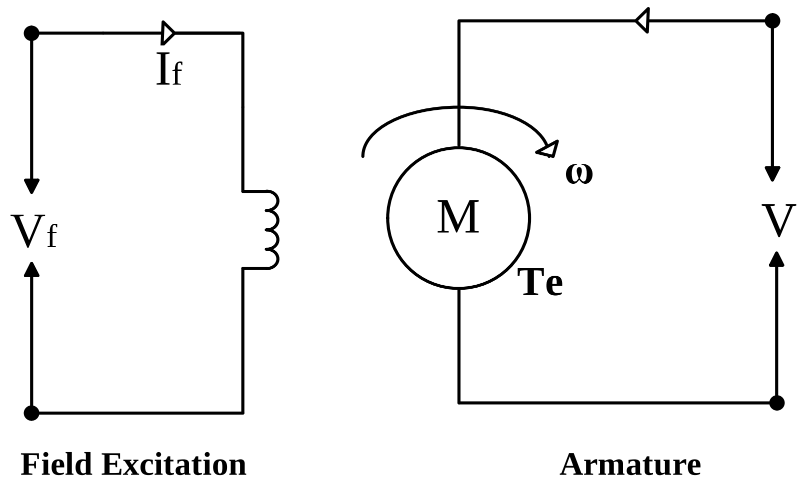

Figure 4.6. Equivalent circuit of Induction motor represented by FOC

The goal of the FOC (also called vector control) on asynchronous machine is to be able to separately control the torque producing and magnetizing flux components. The control technique goal is to (in a sense) imitate the DC motorâĂŹs operation.

4.3.3 Why Field Oriented Control

We know that in the asynchronous machine we face some natural limitations with a V/Hz control approach. FOC control will allow us to get around these limitations, by decoupling the effect of the torque and the magnetizing flux. With decoupled control of the magnetization, the torque producing component of the stator flux can now be thought of as independent torque control. Now, decoupled control, at low speeds, the magnetization can be maintained at the proper level, and the torque can be controlled to regulate the speed.

To decouple the torque and flux, it is necessary to engage several mathematical transforms, and this is where the microcontrollers add the most value. The processing capability provided by the microcontrollers enables these mathematical transformations to be carried out very quickly. This in turn implies that the entire algorithm controlling the motor can be executed at a fast rate, enabling higher dynamic performance. In addition to the decoupling, a dynamic model of the motor is now used for the computation of many quantities such as rotor flux angle and rotor speed. This means that their effect is accounted for, and the overall quality of control is better.

4.3.4 Current Controller and Design

Two motor phase currents are measured. These measurements feed the Clarke transformation module. The outputs of this projection are designated $i_{s\alpha}$ and $i_{s\beta}$. These two components of the current are the inputs of the Park transformation that gives the current in the d,q rotating reference frame. The i_{sd} and i_{sq} components are compared to the references i_{sdref} (the flux reference) and i_{sqref} (the torque reference). Induction motors need a rotor flux creation in order to operate, the flux reference must not be zero.

The torque command i_{sqref} could be the output of the speed regulator when we use a speed FOC. The outputs of the current regulators are V_{sdref} and V_{sqref}; they are applied to the inverse Park transformation. The outputs of this projection are V_{sref} and V_{sref} which are the components of the stator vector voltage in the (α,β) stationary orthogonal reference frame. These are the inputs of the Space Vector PWM. The outputs of this block are the signals that drive the inverter as shown in Fig 4.7. Note that both Park and inverse Park transformations need the rotor flux position. Obtaining this rotor flux position depends on the AC machine type (synchronous or asynchronous machine).

k_p and k_i are parallel PI controller proportional and integral gains respectively. In the series configuration , $k_{p,series}$ sets the gain for all the frequency and $k_{i,series}$ defines the zero point as shown in Fig 4.8. It is known that the gain of the PI controller has a pronounced effect on system stability. But it turns out that the inflection point in the graph also plays a significant but perhaps more subtle role in the performance of the system.

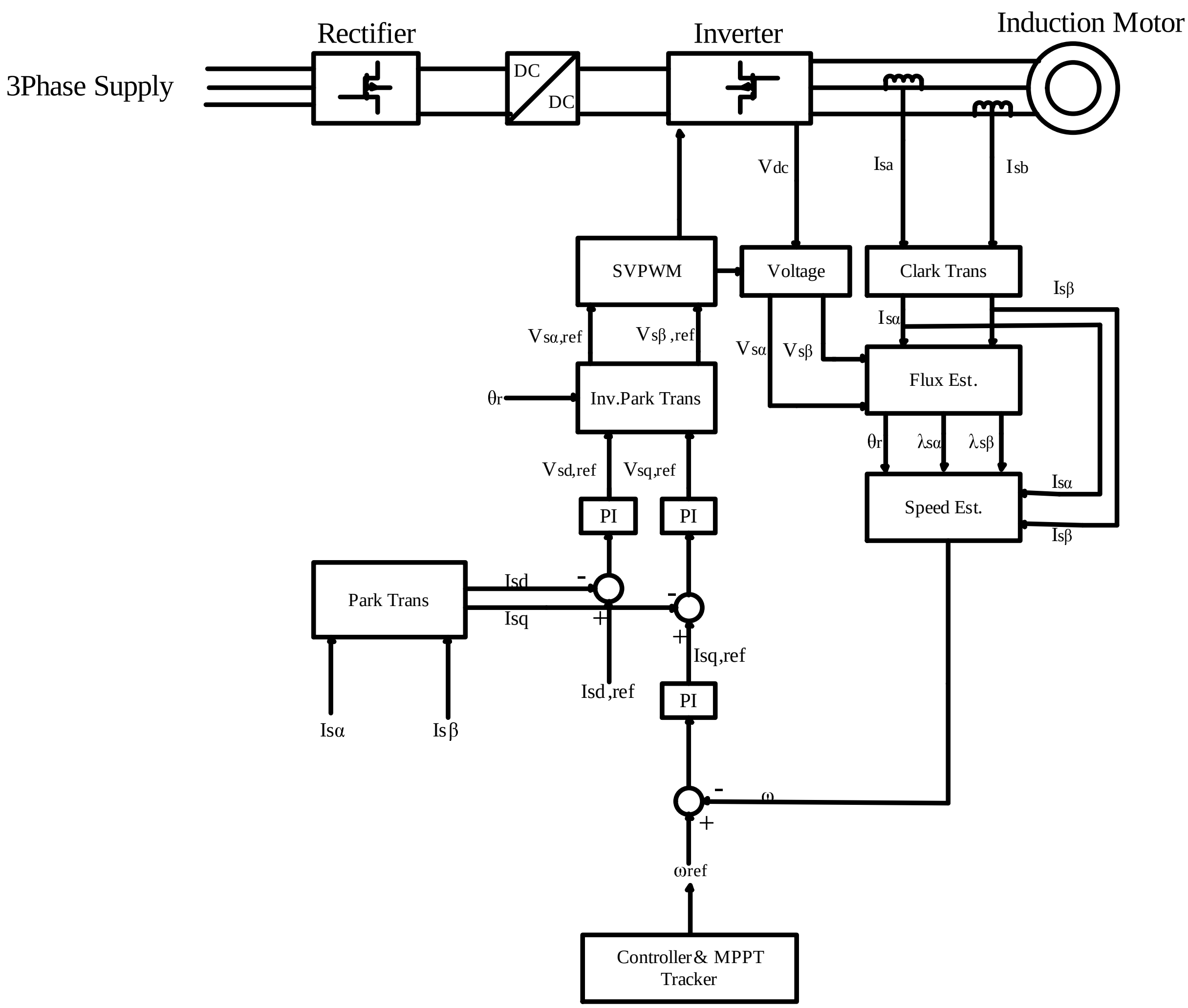

Figure 4.7. FOC control of WTTBS

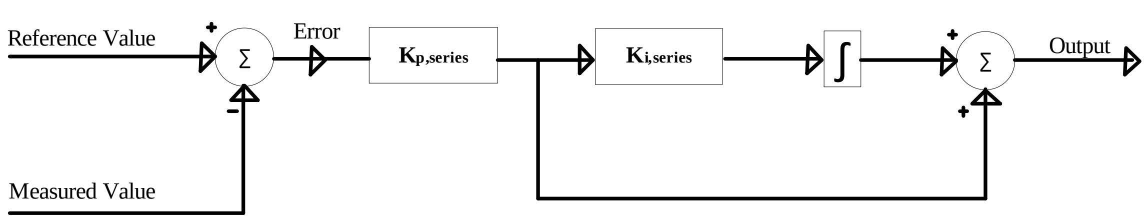

Figure 4.8. Current control PI regulator

$$PI(s) = \frac{k_{p,series}.k_{i,series}}{s} + k_{p,series} \ , \tag{4.15}$$

after rearranging , we get

$$PI(s) = \frac{k_{p,series}.k_{i,series}(1 + \frac{s}{k_{i,series}})}{s} \ . \tag{4.16}$$

By approximating the motor winding to be a simple series circuit containing a resistor, an inductor, and a back-EMF voltage source. We find the total system response by the following closed loop form

$$G(s) = \frac{G_{loop}(s)}{1 + G_{loop}(s)} \ . \tag{4.17}$$

By using (4.8) and (4.9) we get

$$G(s) = \frac{1 + \frac{s}{k_{i,series}}}{(\frac{L}{k_{p,series}}k_{i,series})s^2 + (\frac{R}{k_{p,series}.k_{i,series}} + \frac{1}{k_{i,series}})s + 1} \ . \tag{4.18}$$

4.3.5 Speed Controller and Design

The speed control of an induction motors plays an important role in emulating a wind turbine. The speed controller takes into account the mechanical time constants which effects the stability of the system. The inertia of the motor is the most important parameter required to accurately tune the system. InstaSPIN technology by TI provides the capability to use a very simple but effective technique to quickly tune the PI speed control loop without knowledge of any mechanical parameters.

The stator time constant is much smaller than the mechanical system. Hence the current controller is assumed to be a constant as shown in the Fig 4.9.

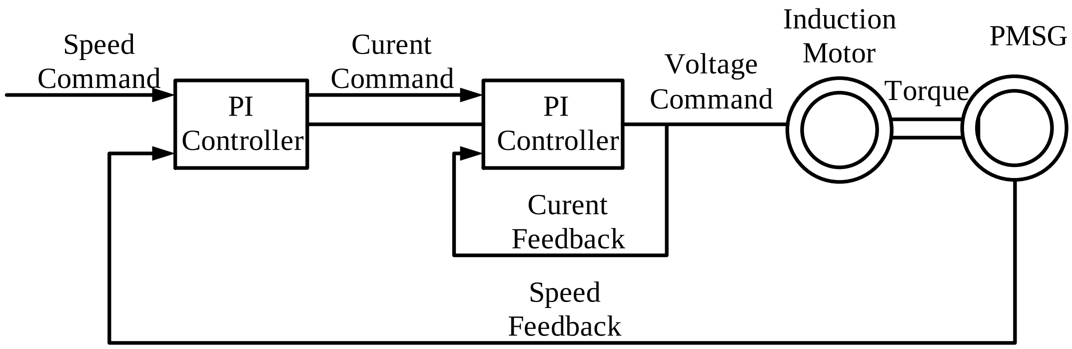

Figure 4.9. Speed Controller

In order to tune the control system , it is required to find out four parameters of the PI controllers . Parameters $k_{p,series}$ and $k_{i,series}$ of current PI control and $sk_{p,series}$ and $sk_{i,series}$ for speed PI controller. Using (4.8) we can write the general form of speed PI controller as follows

$$PI(s) = \frac{sk_{p,series}.sk_{i,series}(1 + \frac{s}{sk_{i,series}})}{s} \ . \tag{4.19}$$

Transfer function of an Induction Motor can be represented by

$$M(s) = \frac{3}{4}P\frac{L_m^2}{L_r}I_d \ . \tag{4.20}$$

The load transfer function is assumed as

$$L(s) = \frac{1}{J}.\frac{1}{s} \tag{4.21}$$

open loop transfer function of the system is

$$GH(s) = \frac{sk_{p,series}.sk_{i,series}(1 + \frac{s}{sk_{i,series}})}{s} \times \frac{1}{\frac{L}{k_{i,series}}s + 1} \times \frac{3}{4}P\frac{L_m^2}{L_r}I_d \times \frac{1}{J}\frac{1}{s} \tag{4.22}$$

assuming k_{const} as $\frac{3}{4}\frac{PL_m}{JL_r}$

we get

$$GH(s) = \frac{k_{const} \times sk_{p,series}.sk_{i,series}(1 + \frac{s}{sk_{i,series}})}{s^2(1 + \frac{L}{k_{p,series}s})} \ . \tag{4.23}$$

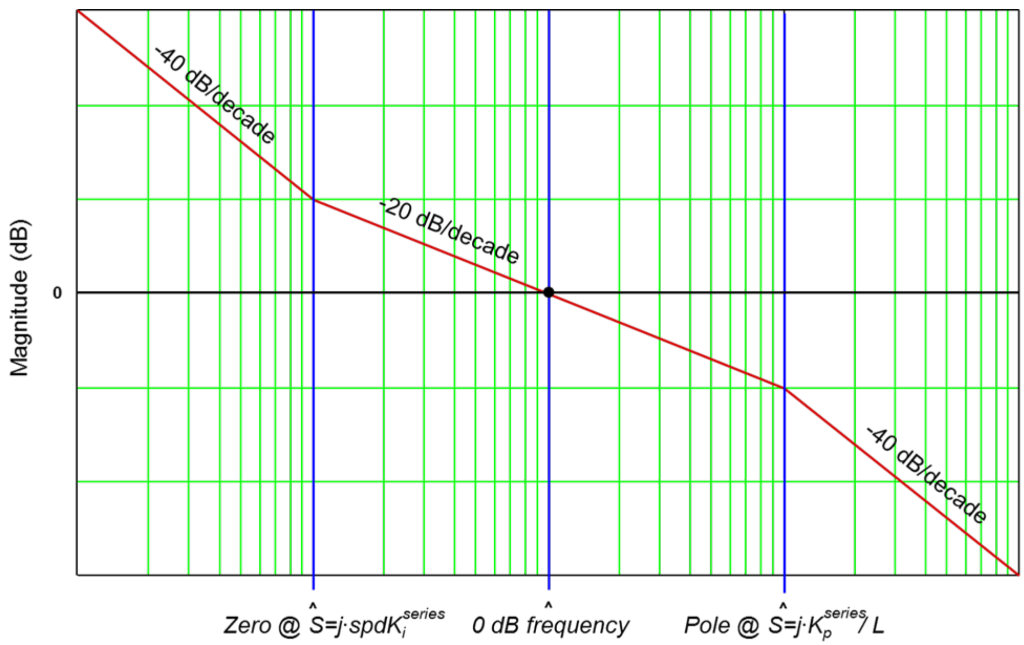

Figure 4.10. Bode Plot of the tuned controller[Instaspinlab]

4.4 3p Oscillations

The fluctuations in the electrical power output of a wind turbine generator are predominantly caused by Tower shadow and Wind sheer effects. The frequency of the periodic fluctuations is n times the blade rotational frequency p, where n is the number of blades. For three-bladed wind turbines, this inherent characteristic is known as the $3p$ effect.

4.4.1 Wind Sheer

Wind turbine blades experiences maximum wind speed when facing directly upwards and minimum when the blades are facing downwards. This variation in wind with height is known as wind shear. For three-bladed wind turbines, each of the three blades will experience minimum wind speed in one complete rotation and hence wind shear contributes to the $3p$ frequency [43]. The hub spead is given by

$$v = v_H(\frac{z}{H})^{\alpha} \ , \tag{4.24}$$

where z, H, v_h, and α are the elevation above ground, hub height, wind speed at hub height, and empirical wind shear exponent respectively. For the purpose of this analysis, Eqn.(4.24) is converted to a function of r (radial distance from rotor axis) and θ (azimuthal angle) [44] as given by

$$v(r,\theta) = v_H(\frac{rcos\theta + H}{H})^{\alpha} = v_H[1 + w_s(r,\theta)] \ , \tag{4.25}$$

where v_H is the wind speed at hub height, r is the radial distance from rotor axis, w_s is the wind-shear-shape function [18], α is the empirical wind shear exponent, h is the elevation of rotor hub, and z is the elevation above ground. The term $w_s(r,)$ is the disturbance seen in wind speed due to wind shear that is added to hub height wind speed. According to [44] $w_s(r,\theta)$ can be approximated by a third order truncated taylor series as given by

$$w_s(r,\theta) \approx \alpha(\frac{r}{H})cos\theta + \frac{\alpha(\alpha-1)}{2}(\frac{r}{H})^2 cos^2\theta + \frac{\alpha(\alpha-1)(\alpha-2)}{6}(\frac{r}{H})^3 cos^3\theta \ . \tag{4.26}$$

4.4.2 Tower Shadow

Tower shadow effect alters the uniform flow of wind due to the presence of the tower. For an upwind turbine, the blade is directly in front of the tower, hence it torque at each blade is reduced. This is called tower shadow effect. A three-bladed wind turbine blades experiences minimum wind in one complete rotation and hence tower shadow contributes to the 3p effect. This section models tower shadow effect for an upwind turbine and identifies the factors affecting it. The spatial velocity can be obtained by

$$\phi = \phi_{uniform} + \phi_{doublet} \text{ and} \tag{4.27}$$

$$= v_H y(1 - \frac{a^2}{x^2 + y^2}) \ . \tag{4.28}$$

Differentiating stream function ϕ with respect to y yields the total wind flow velocity v(y, x) in the x-direction as

$$v(y, x) = v_H + v_{tower}(y, x) \ , \tag{4.29}$$

$$v_{tower}(y, x) = v_0 a^2 \frac{y^2 - x^2}{x^2 + y^{2^2}} \ , \tag{4.30}$$

where v_0 is the spatial velocity.

$$v_{tower}(r, \theta, x) = v_h a^2 \frac{r^2 sin\theta^2 - x^2}{(r^2 sin\theta^2 + y^2)^2}, . \tag{4.31}$$

Eqn.(2.8) is valid for tower shadow zone, that is, 90deg $< \theta <$ 270deg . Here, the hub velocity v_H is assumed to be equal to spatial velocity v_0.

4.5 Simulation Results

The WECS considered for system design consist of a 8500 W wind turbine rated at 13 m/s coupled to a PMSG. For the design of WTTBS, the wind turbine model is replaced by an induction motor of 5.5 kW.

4.5.1 Test Bench Emulation

The behavior of wind energy conversion system has been tested and analyzed for two scenarios. Scenario 1, Fig 4.11, emulates WECS with a wind turbine connected to PMSG and a load for 4 m/s windspeed. Scenario 2, Fig 4.12, emulates the same WECS configuration, but this time with an intelligent Induction motor drive instead of wind turbine. The initial disturbance in DC bus voltage indicate the presence of $3p$ oscillations as shown in scenario 2. The results of both the scenarios are compared. The PMSG is connected to the grid through a DC link capacitor. Fig 4.13 demonstrates the variation of system parameters for dynamic wind change.

The results in Fig 4.13 also demonstrates the variation of Induction motor drive parameters with change in windspeed. Excellent similarity is observed between the simulation results of scenario 1 and scenario 2 which proves that WTTBS replicates the characteristics of a real wind turbine and wind turbine can be replaced by a WTTBS for laboratory emulation.

4.5.2 Computation Parameters

Table 4.2. Mechanical System Parameters

Parameter	Value
Rated PMSG power	9.1 kW
No. of Pole pairs	5
PMSG inertia	0.87 kg m^2
Rated Induction motor power	5.5 kW
Induction Motor inertia	0.089 kg m^2
Wind turbine rated power	8.2 kW
Wind turbine inertia	128 kg m^2
Area of the blade	5.89 m^2
Rated turbine rotor speed	43.24 rad/sec

Table 4.3. ω_{opt} and $P_{mech,max}$ for various windspeeds

Windspeed	ω_{opt}[rad/sec]	$P_{mech,max}$[kW]	$Torque$[N-m]
3	10.78	126.3	11.7
4	14.44	299.3	20.7
5	18.00	584.5	32.4
6	21.56	1010.0	46.8
7	25.23	1603.9	63.5
8	28.79	2394.1	83.1
9	32.35	3406.8	105.3

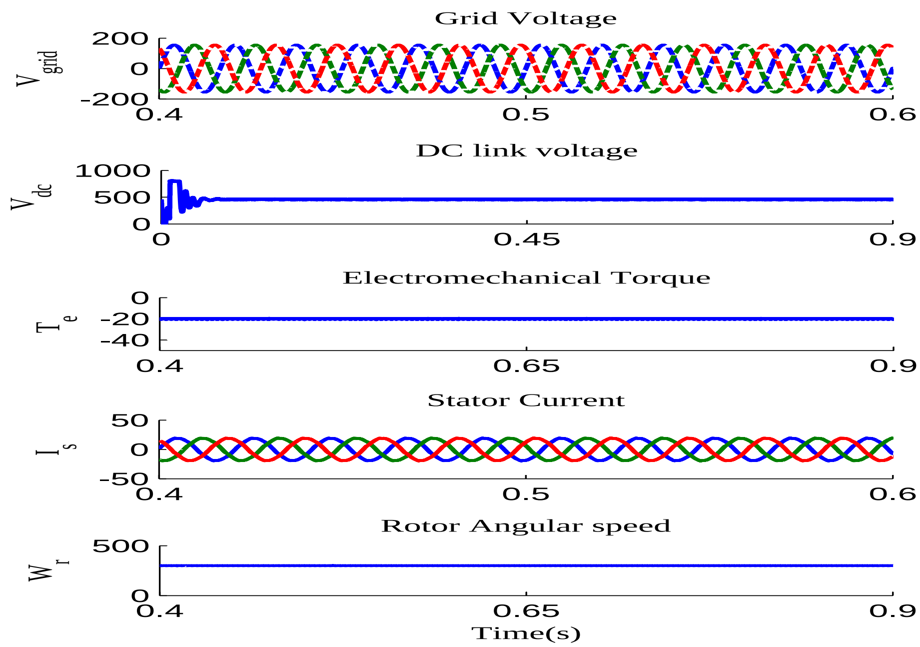

Figure 4.11. Simulation results for Scenario 1

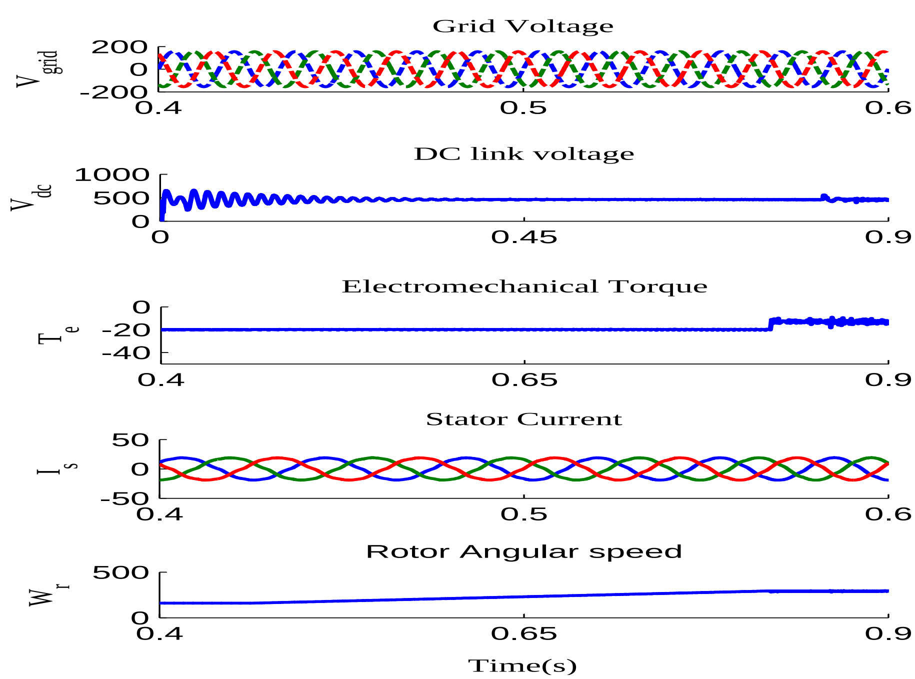

Figure 4.12. Simulation results for Scenario 2

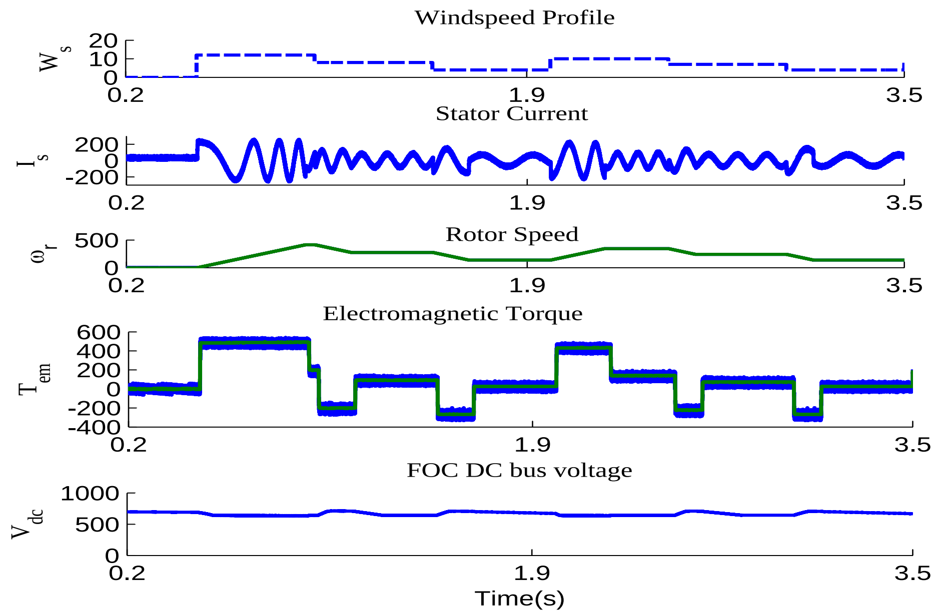

Figure 4.13. Emulator with varied Windspeed

4.5.3 Wind Sheer properties

From (4.24) and (4.25), it can be seen that disturbance in wind caused by wind shear is dependent mainly on V_H, H, α and r. Fig 4.14 shows the variation of wind shear with wind velocity at hub height (v_H). For V_h = 12 m/s, the maximum wind speed experienced by the blades of a wind turbine is 13 m/s when the azimuthal angle (θ) is at 0 , while the minimum wind speed is 12.4 m/s occurs when the azimuthal angle (θ) is at 180. Hence, the variation in wind speed, that is, the difference between maximum and minimum wind speed for one complete blade rotation is 0.6 m/s. Similarly for v_h = 11.5 m/s, the variation in wind speed is 0.5 m/s. Thus wind shear increases with the increase in v_h.

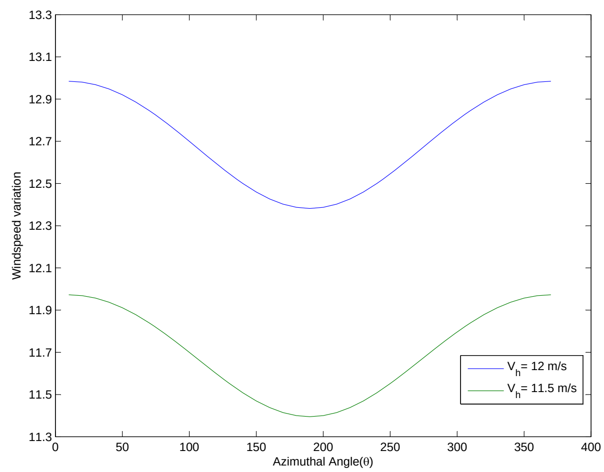

Figure 4.14. Wind speed variation vs Azimuthal angle for various hub velocity

Fig 4.15 shows the impact of α on wind shear. The values of α have been chosen depending on terrain, as shown in (Table 1) [12]. Increase in α increases wind sheer. Fig 4.16 shows that wind shear decreases with increase in hub height. For example, at H = 170 m, the variation in wind is 0.05 m/s while at H = 50 m, the wind variation is 0.6 m/s. Fig 4.17 shows the wind shear experienced by different blade elements. Minimum wind shear is experienced by the blade element closest to the hub (r = 2.5 m).

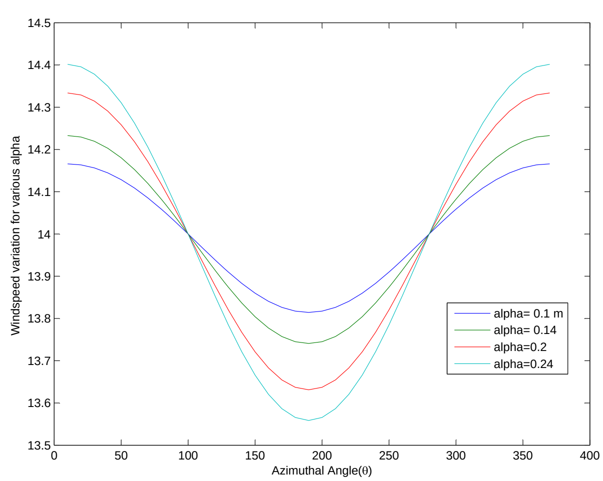

Figure 4.15. Wind speed variation vs Azimuthal angle for various α

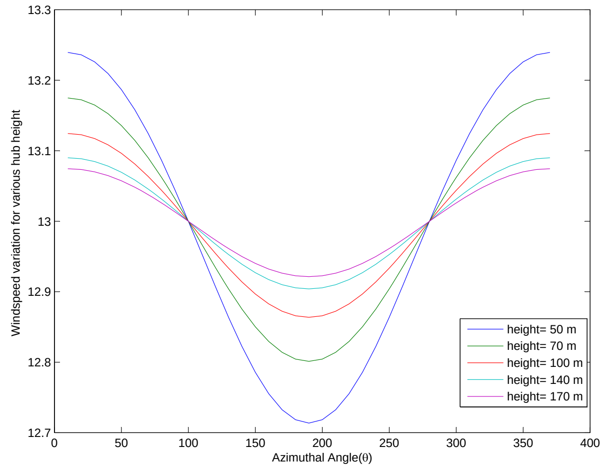

Figure 4.16. Wind speed variation vs Azimuthal angle for various heights

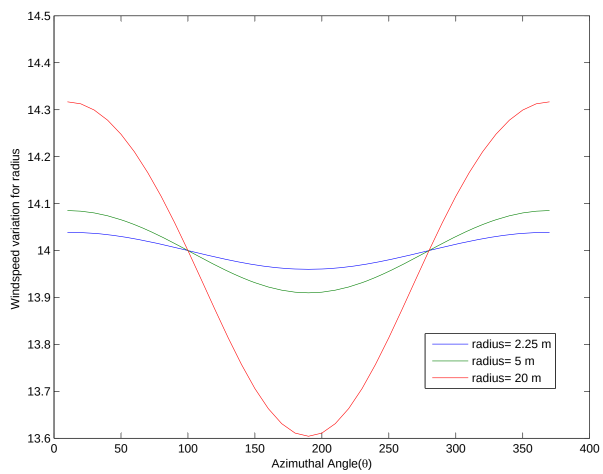

Figure 4.17. Wind speed variation vs Azimuthal angle for various radial distance

4.5.4 Tower Shadow Properties

From (4.30), it is observed that the disturbance in wind due to tower-shadow effect depends predominantly on three factors, r, θ, and x. Fig 4.19 demonstrates how change in r from 5m to 20 m in (6) with change in azimuthal angle θ effects the wind velocity. It should be noted that tower shadow angle varies from 90deg $< \theta <$ 270deg . It is observed that the blade elements closest to the hub (r = 5 m) experience a longer duration of the tower shadow. However at θ = 180deg, that is, blade directly in front of the tower, the same wind deficit is seen by all the blade elements. Next, the radial distance of blade element from the hub, that is, r is kept constant at 10 m and the distance of blade origin from the tower midline, that is, x is varied from 2m to 5 m. As seen from Fig 4.20, the tower shadow effect is most pronounced when the blades are closer to the tower (x = 2 m). Hence, mounting the blades away from the tower minimizes tower-shadow effects

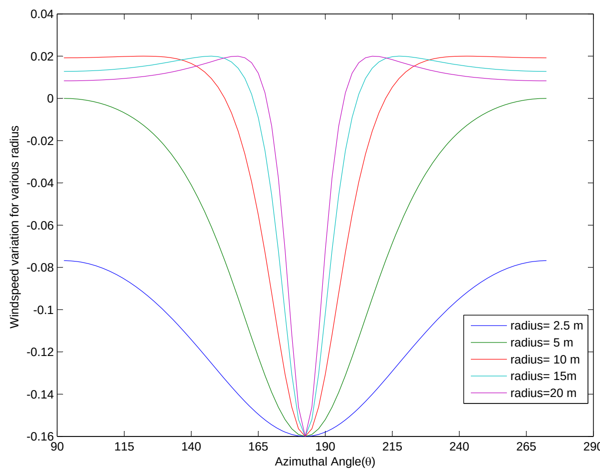

Figure 4.18. Wind speed variation vs Azimuthal angle for various radius

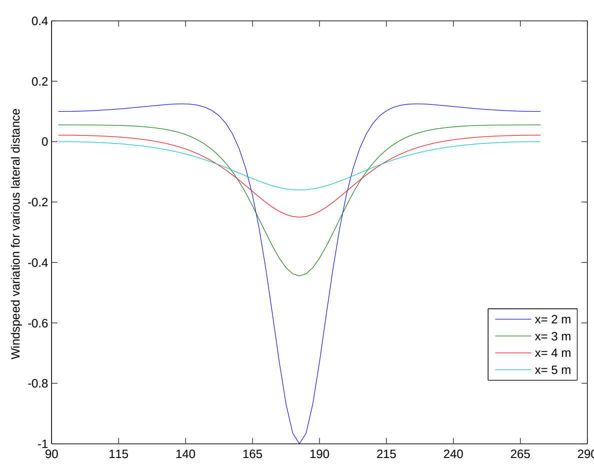

Figure 4.19. Wind speed variation vs Azimuthal angle for various heights

Chapter 5 Experimental Result

Power conditioning Units (PCU) plays a major role in processing the power required for specific applications. Over the past few years Micro-controllers based PCUs are used for implementing complex algorithms and mathematical calculations. A number of high power PCUs can be controlled with the help of a single micro-controller. Amongst these, Digital Signal Processing (DSP) micro-controllers are gaining popularity in control of PCUs because of their capability to handle large amount of data. This chapter gives a detailed description of the use of DSP micro-controller for implementing the objective of this thesis. The hardware setup is described. TMS320F28069M (InstaSPIN-MOTION or InstaSPIN-FOC) control card is placed on a High voltage motor control kit for an actual implementation for a conventional wind system . The results have been presented and compared.

5.1 Use of DSP Micro-controllers for PCUs

The use of DSP micro-controllers has moved from support to the existing main control system to being the actual control system. Power electronics applications require more advanced features and functionality which need to be incorporated in control systems in order to reduce their size and cost. DSP micro-controllers allows automotive and industrial motor drives control to be advanced and cost effective. Other advantages of DSP include higher speed to handle high frequency inputs. PCUs require advanced PWM based control and complicated algorithms. There is a need for precise and reliable control with provisions for protecting critical parts of the system in case of faults. Digital signal processors (DSP) play an important role for implementing such control methods since their operating speeds are very high which ensure fast response times to faults. Also being reprogrammable, changes to the control can easily be made in case any changes to the control part of the system need to be made. Advantages of DSP processor power control over analog methods are

- Precision
- High Reliability
- High Speeds
- Ease of implementation of Multiplication and Square root
- Low cost and size

5.2 Code Composer Studio

TI's Code Composer Studio (CCS) is an Integrated Development Environment (IDE). It is used for the development of all the phases: coding the micro-controller, editor in C, linker, assembler, interface to load the program on the micro-controller as well as debugger. It also has advanced features such as real time data exchange. CCS provides a friendly environment for managing files and projects. Various library files have been provided with definitions for standardized functions and with initializations and other standard routines for different modules. CCS comes with an editor, a compiler, an assembler and a linker. The source files can be in assembly or C. CCS provides support tools like watch windows, break points and probe points, single stepping through the code, real time monitoring tools, memory watch, etc. The variety of graphical data formats allows us to the real time capabilities supported by CCS. Not just the graphical displays, all the debug windows (watch windows and memory windows) can be continuously refreshed in real time. This power to look into your application in real time,vwhile your system is running, is invaluable. This provides the system designer an opportunity to optimize his/her system for the real world.

5.3 High Voltage Motor Control kit

Figure 5.1. Motor control kit

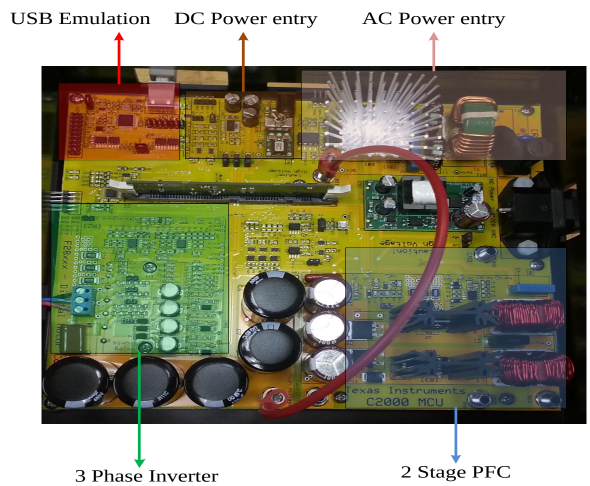

Figure 5.2. Power stages in the HV kit

The High Voltage Digital Motor Control (DMC) and Power Factor Correction (PFC) kit (TMDSHVMTRPFCKIT), provides a great way to research with digital control of high voltage motors and to use PFC to increase efficiency of operation.

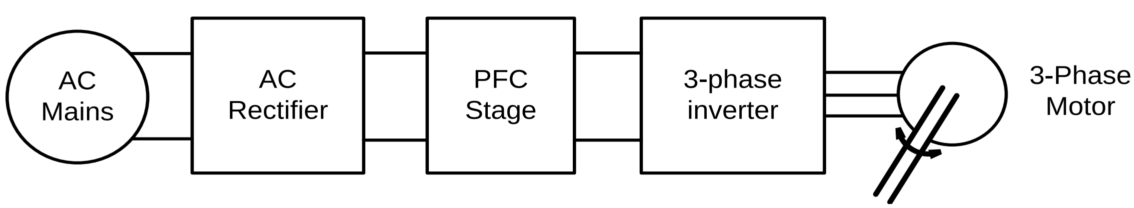

Figure 5.3. High Voltage Motor Control Kit block diagram

Fig 5.1 gives a block diagram of different stages present on the High voltage motor control kit to power from the induction motor. The input to the kit is a 15V DC power supply which powers the controller and the supporting circuitry and an AC input (85-132VAC/ 170-250VAC) to run the motor. The High Voltage DMC board if fitted inside a plastic enclosure. A heat sink is mounted underneath the board to the motor inverter and a DC Fan is attached to this heat sink to increase airflow. The board can accept any of the C2000 series controlCARDs. A F28035 and F28335 control card is typically with the kit. Different power stages used on the kit are

5.3.1 3 Phase Inverter

- 350V DC max input voltage
- 1 kW/1.5 kW maximum load (for > 250 W load, the fan attached to the IPM heatsink is used)
- Sensorless and Sensored Field Oriented Control of ACI Motor

5.3.2 PFC Stage

Two phase interleaved topology, capable of phase shedding

- 85-132VAC/ 170-250VAC rectified input
- 400V DC Max output voltage
- 750W max power rating
- Up to 96 % efficiency
- 200Khz switching frequency for the power stage
- Upto 100Khz PFC control loop frequency

5.3.3 AC rectifier

This stage is rated for delivering up to 750W power. This stage can be used to either generate the DC Bus voltage for the inverter directly or provide input for the Power Factor Correction stage present on the board.

- 85-132VAC/ 170-250VAC input
- 750W max power rating

5.4 Results

The described wind turbine test bench system has been implemented and tested in our laboratory. The wind turbine model and the digital PI controller are realized using a PC loaded with Code Composer Studio interfaced to the high voltage motor control kit. The FOC controller generates the current and frequency demands for the IGBT inverter. In this research, a horizontal axis wind turbine as described in the previous section is used. The parameters of the IM are listed in Table 4.2. Fig 5.2 through 5.9 verify that the developed wind turbine simulator reproduces the steady-state characteristics of a given wind turbine under several wind profiles. The torque response of a WTTBS simulating a 8.5-kW in software is scaled down to 1/4HP in the hardware implementation. Fig 5.4 clearly shows the torque of the motor under a constant windspeed. Fig 5.5 through 5.7 shows the WTTBS response for a constant wind speed. When there is a step change in the windspeed (user input in the Code Composer Studio software), the IM changes its torque as shown in Fig 5.8. Fig 5.9 through 5.11 shows the variation of system parameters under variable wind speed conditions.

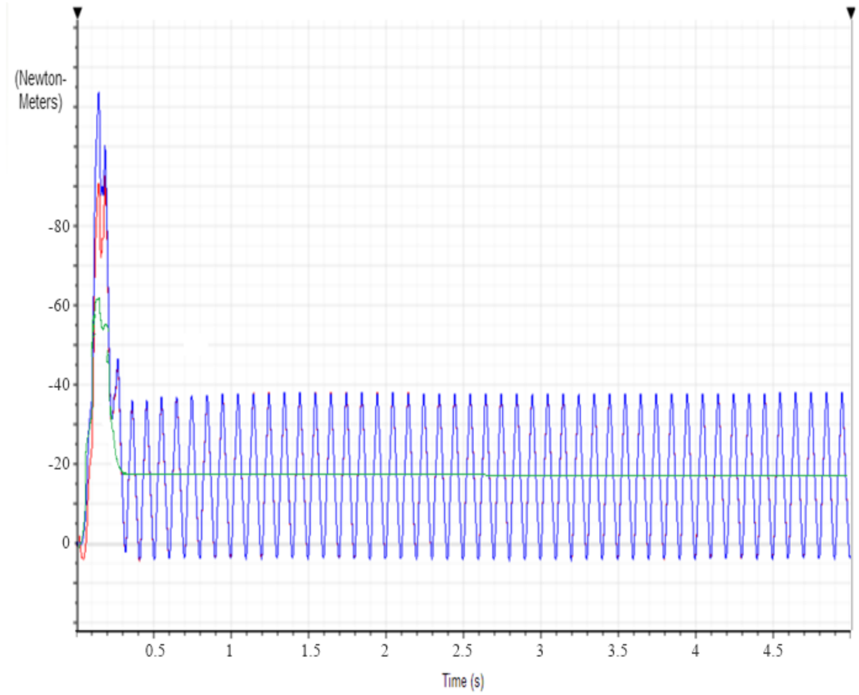

Figure 5.4. Torque generated by the controller under a constant windspeed (N-m)

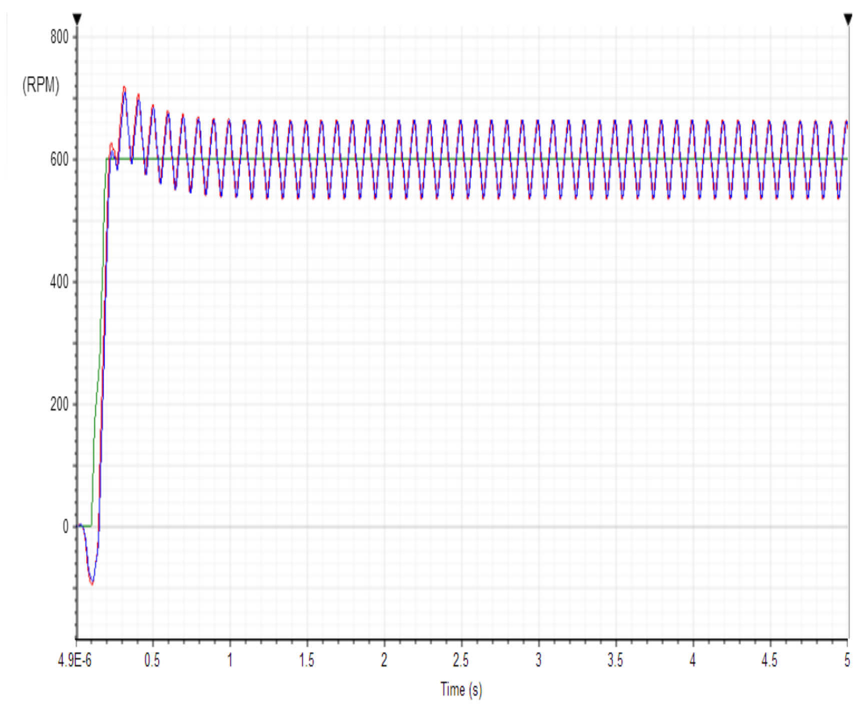

Figure 5.5. Rotor speed of the induction motor under constant windspeed (RPM)

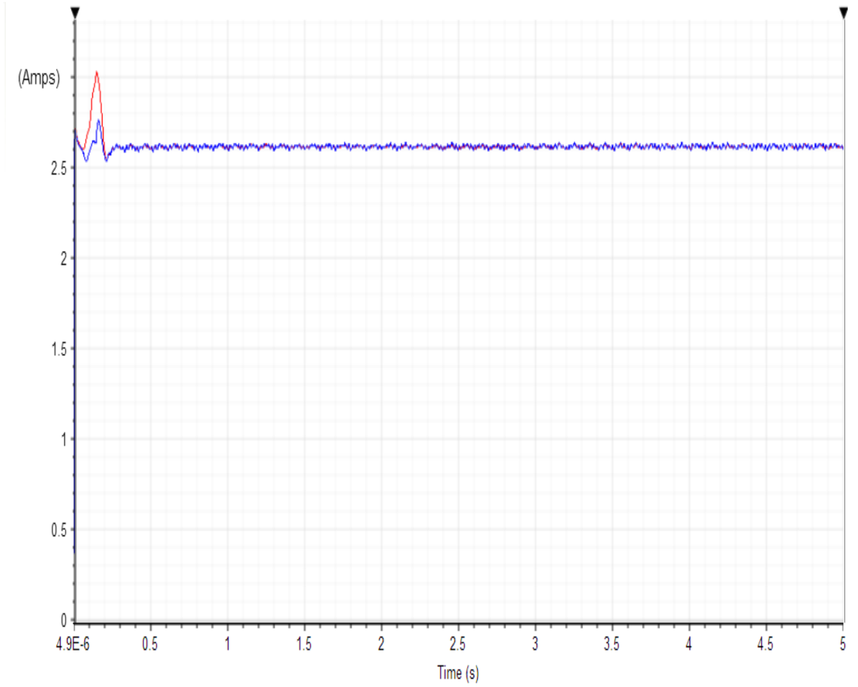

Figure 5.6. i_d Current generated by controller for a constant windspeed (A)

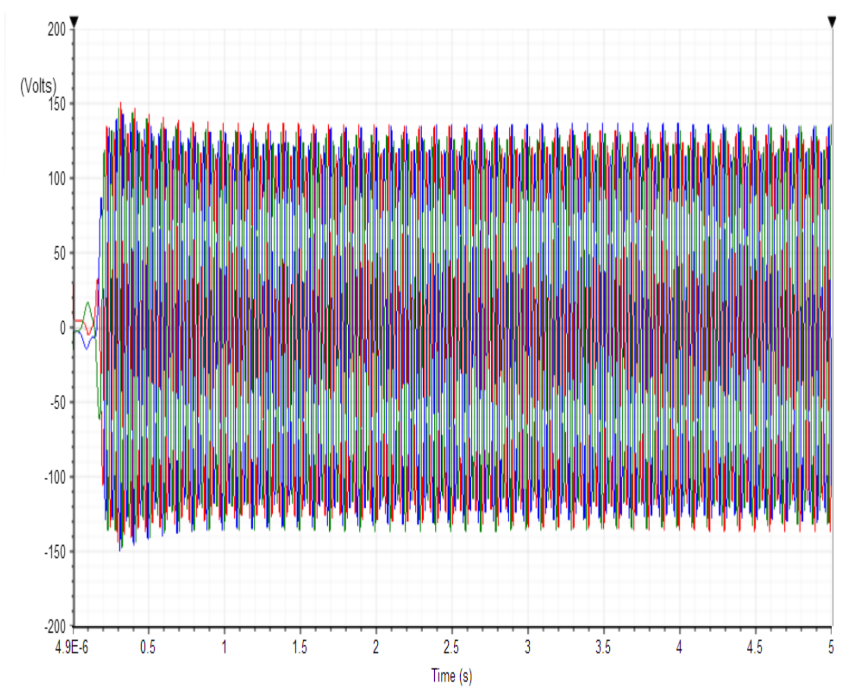

Figure 5.7. Voltage of the induction motor for a constant windspeed (volts)

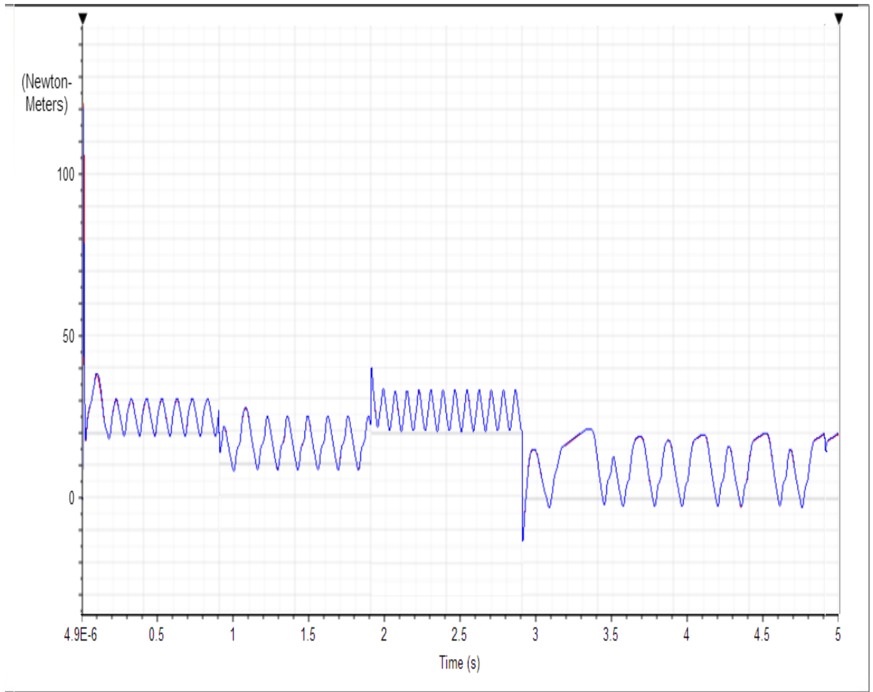

Figure 5.8. Torque generated by the controller under a variable windspeed (N-m)

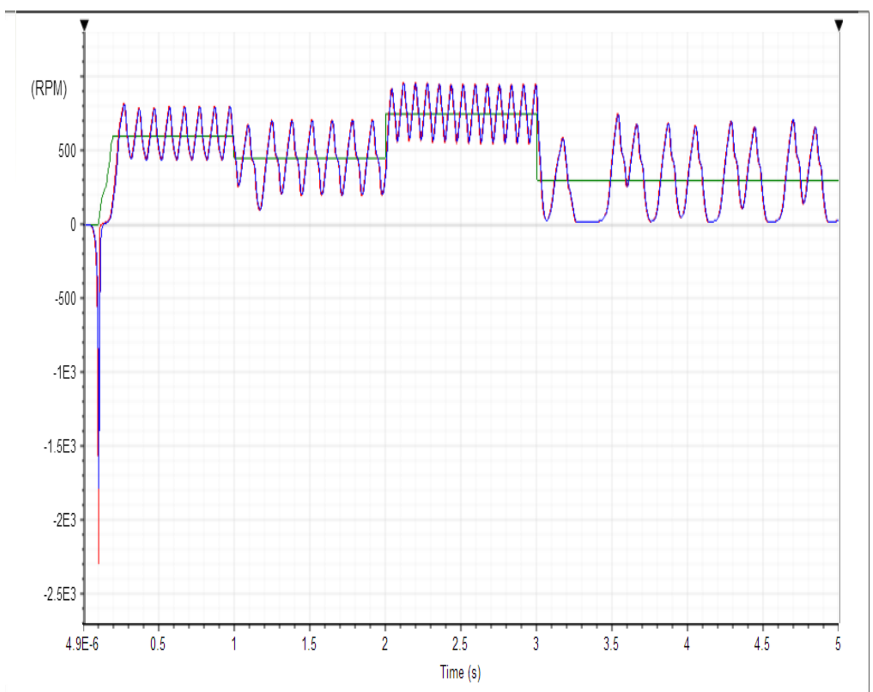

Figure 5.9. Rotor speed of the induction motor under variable windspeed (RPM)

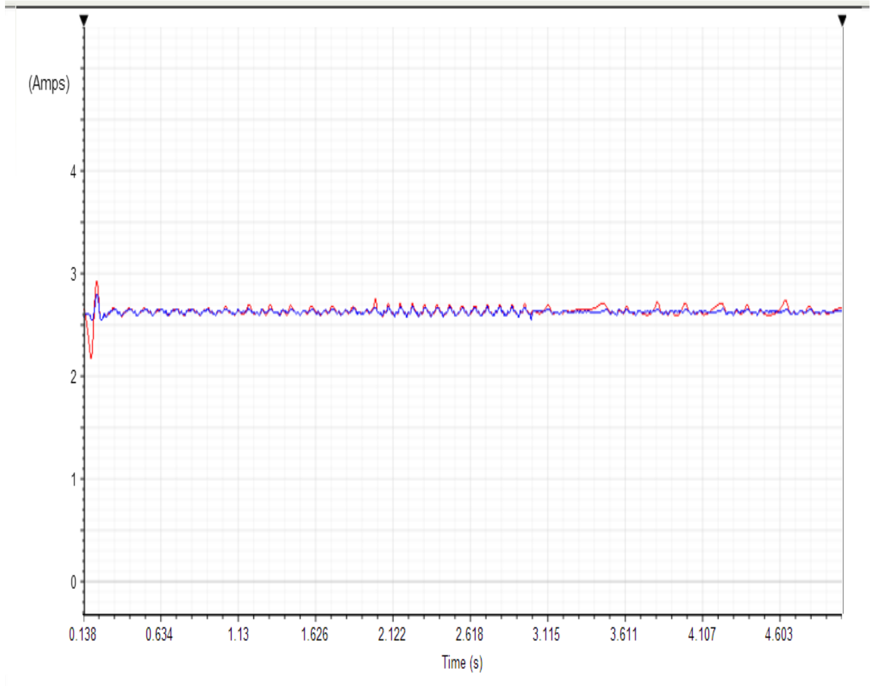

Figure 5.10. i_d Current generated by controller for a variable windspeed (A)

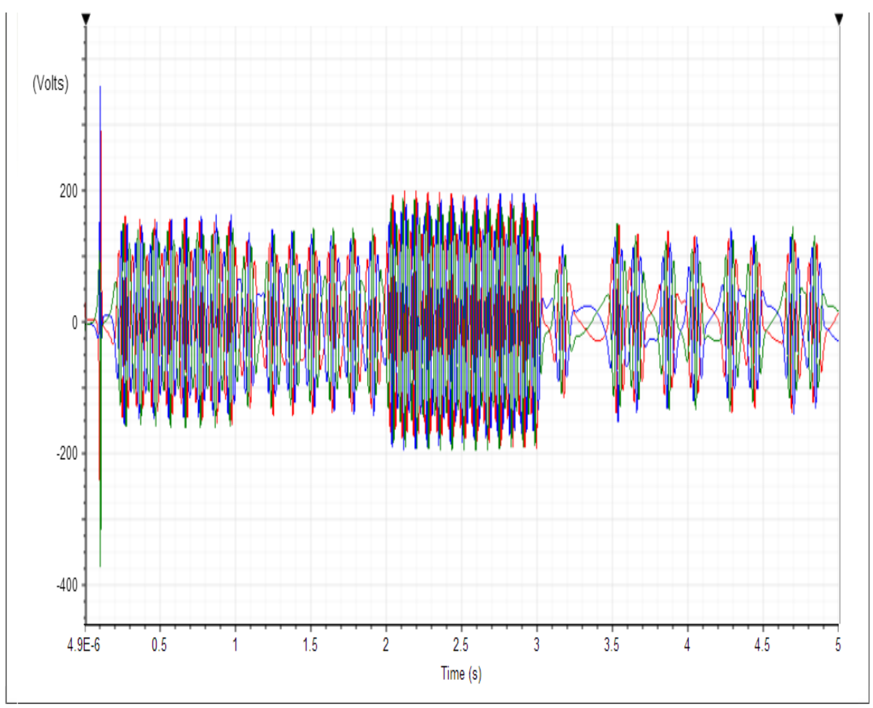

Figure 5.11. Voltage of the induction motor for a variable windspeed (volts)

Chapter 6 Conclusions and Future Work

6.1 Conclusion

The research proposed in this thesis aims at maximizing the efficiency of the wind energy conversion system by accurately predicting the Maximum Power Point (MPP). The conventional Hill climbing method relies on the perturbation step size for the accurate tracking of MPP. This causes the speed-efficiency tradeoff problem. The extracted average output power by the conventional MPPT techniques is drastically reduced due to these oscillations around the MPP.

A two step MPPT technique has been proposed that addresses the problems that exist in the conventional hill-climbing. The proposed controller initially detects the optimal cubic power curve by deriving the optimal duty ratio from the boost chopper generation control. This curve is used as a reference for the novel point search method to converge to the MPP. The point search method regulates the duty ratio of the boost converter (D) in an iterative fashion till the operating reaches the MPP along the optimal power curve.

An accurate wind turbine model is defined and the proposed MPPT controller has been analytically proved for this model. A summary of mathematical analysis pertaining to duty cycle time variations is presented to justify the effectiveness of the proposed method in mitigating the power loss in the WECS. Simulated results for the proposed algorithm and hill climbing method are compared in terms of the tracking time and accuracy of convergence. It is found that the proposed method tracks the MPP at a faster rate than the hill climbing method.

A Wind Turbine Test Bench System has been designed to emulate the characteristics of a real wind turbine. It was deduced during the research that Field oriented control of an induction motor would provide robust and cost effective method to replicate the static and dynamic characteristics of a wind turbine systems. Wind Turbine Test Bench System was designed to emulate a 8kW PMSG wind turbine. The simulation results confirms the validity of the proposed test bench system. A 1/4 HP scaled down version of High voltage motor control kit was used to justify the results. Hardware implementation of WTTBS corroborates the simulation results

6.2 Future work

Design and development of WECS necessitates the need of detailed design processes to determine the best configuration, suitable location and a MPPT method, all of which requires numerous on site experiments. Hence an accurate Wind Turbine Test Bench System (WTTBS) can be effectively used to validate the design of laboratory concept prototypes. The bench system proposed in this thesis has to be integrated with the designed MPPT controller so that the entire system can be emulated in the laboratory.

References

[1] NRDC. (2009, Jun.) Renewable energy of america. [Online]. Available: http://www.nrdc.org/energy/renewables/wind.asp

[2] AWEA. (2012, Jun.) Awea 4th quarter 2012 public market report". [Online]. Available: http://www.fws.gov/southwest/es/documents/R2ES/LitCited/LPC_2012/AWEA_2012a.pdf

[3] R. Doe. (2013, Jun.) This is a test entry of type @ONLINE. [Online]. Available: AWEA4thquarter2013PublicMarketReport".AmericanWindEnergyAssociation

[4] D. S. Mathew, "Wind energy," *Springer Berlin Heidelberg*, 2008.

[5] M. Huleihil, "Maximum windmill efficiency in finite time," *Journal of Applied Physics*, vol. 105, no. 10, pp. 104 908–104 908–4, May 2009.

[6] J. Hui, "An adaptive control algorithm for maximum power point tracking for wind energy conversion systems," *Queens University*, December 2008.

[7] H. Jafarnejadsani, J. Pieper, and J. Ehlers, "Adaptive control of a variable-speed variable-pitch wind turbine using radial-basis function neural network," *Control Systems Technology, IEEE Transactions on*, vol. 21, no. 6, pp. 2264–2272, Nov 2013.

[8] windpower.org, December 2006.

[9] S. Heier, "Grid integration of wind energy conversion systems," May 1998.

[10] M. Idan, D. Lior, and G. Shaviv, "A robust controller for a novel variable speed wind turbine transmission," *Journal of Solar Energy Engineering*, vol. 120(4), pp. 247–252, Jan 1998.

[11] Y. Song, D. Dhinakaran, and X. Bao, "Variable speed control of wind turbines using nonlinear and adaptive algorithms," *Journal of Wind Engineering and Industrial Aerodynamics*, vol. 120(4), pp. 247–252, Jan 2000.

[12] S. Raza Kazmi, H. Goto, H.-J. Guo, and O. Ichinokura, "A novel algorithm for fast and efficient speed-sensorless maximum power point tracking in wind energy conversion systems," *Industrial Electronics, IEEE Transactions on*, vol. 58, no. 1, pp. 29–36, Jan 2011.

[13] N. Femia, G. Petrone, G. Spagnuolo, and M. Vitelli, "Optimization of perturb and observe maximum power point tracking method," *Power Electronics, IEEE Transactions on*, vol. 20, no. 4, pp. 963–973, July 2005.

[14] P. Huynh and B. H. Cho, "Design and analysis of a microprocessor-controlled peak-power-tracking system [for solar cell arrays]," *Aerospace and Electronic Systems, IEEE Transactions on*, vol. 32, no. 1, pp. 182–190, Jan 1996.

[15] J. Yaoqin, Y. Zhongqing, and C. Binggang, "A new maximum power point tracking control scheme for wind generation," in *Power System Technology, 2002. Proceedings. PowerCon 2002. International Conference on*, vol. 1, Oct 2002, pp. 144–148 vol.1.

[16] E. Muljadi, S. Drouilhet, R. Holz, and V. Gevorgian, "Analysis of permanent magnet generator for wind power battery charging," in *Industry Applications Conference, 1996. Thirty-First IAS Annual Meeting, IAS '96., Conference Record of the 1996 IEEE*, vol. 1, Oct 1996, pp. 541–548 vol.1.

[17] K. Amei, Y. Takayasu, T. Ohji, and M. Sakui, "A maximum power control of wind generator system using a permanent magnet synchronous generator and a boost chopper circuit," in *Power Conversion Conference, 2002. PCC-Osaka 2002. Proceedings of the*, vol. 3, 2002, pp. 1447–1452 vol.3.

[18] J. Thongam, P. Bouchard, R. Beguenane, A. Okou, and A. Merabet, "Control of variable speed wind energy conversion system using a wind speed sensorless optimum speed mppt control method," in *IECON 2011 - 37th Annual Conference on IEEE Industrial Electronics Society*, Nov 2011, pp. 855–860.

[19] Q. Wang and L. Chang, "An intelligent maximum power extraction algorithm for inverter-based variable speed wind turbine systems," *Power Electronics, IEEE Transactions on*, vol. 19, no. 5, pp. 1242–1249, Sept 2004.

[20] H. Li, K. L. Shi, and P. McLaren, "Neural-network-based sensorless maximum wind energy capture with compensated power coefficient," *Industry Applications, IEEE Transactions on*, vol. 41, no. 6, pp. 1548–1556, Nov 2005.

[21] A. Abo-Khalil, D.-C. Lee, and J.-K. Seok, "Variable speed wind power generation system based on fuzzy logic control for maximum output power tracking," in *Power Electronics Specialists Conference, 2004. PESC 04. 2004 IEEE 35th Annual*, vol. 3, June 2004, pp. 2039–2043 Vol.3.

[22] E. Koutroulis and K. Kalaitzakis, "Design of a maximum power tracking system for wind-energy-conversion applications," *Industrial Electronics, IEEE Transactions on*, vol. 53, no. 2, pp. 486–494, April 2006.

[23] M. Matsui, D. Xu, L. Kang, and Z. Yang, "Limit cycle based simple mppt control scheme for a small sized wind turbine generator system-principle and experimental verification," in *Power Electronics and Motion Control Conference, 2004. IPEMC 2004. The 4th International*, vol. 3, Aug 2004, pp. 1746–1750 Vol.3.

[24] S. Wang, Z. Qi, and T. Undeland, "State space averaging modeling and analysis of disturbance injection method of mppt for small wind turbine generating systems," in *Power and Energy Engineering Conference, 2009. APPEEC 2009. Asia-Pacific*, March 2009, pp. 1–5.

[25] J.-M. Kwon, J. H. Kim, S.-H. Kwak, and H.-H. Lee, "Optimal power extraction algorithm for dtc in wind power generation systems," in *Sustainable Energy Technologies, 2008. ICSET 2008. IEEE International Conference on*, Nov 2008, pp. 639–643.

[26] R.-J. Wai and C.-Y. Lin, "Implementation of novel maximum-power- extraction algorithm for pmsg wind generation system without mechanical sensors," in *Robotics, Automation and Mechatronics, 2006 IEEE Conference on*, Dec 2006, pp. 1–6.

[27] S. W. Mohod and M. V. Aware, "Laboratory development of wind turbine simulator using variable speed induction motor," *International Journal of Engineering, Science and Technology*, vol. 3, no. 5, pp. 73–82, Jan 2011.

[28] Y. Jia, Z. Wang, and Z. Yang, "Experimental study of control strategy for wind generation system," in *Power Electronics Specialists Conference, 2007. PESC 2007. IEEE*, June 2007, pp. 1202–1207.

[29] H. Kojabadi, L. Chang, and T. Boutot, "Development of a novel wind turbine simulator for wind energy conversion systems using an inverter-controlled induction motor," *Energy Conversion, IEEE Transactions on*, vol. 19, no. 3, pp. 547–552, Sept 2004.

[30] M. N. Mansouri, M. F. Mimouni, B. Benghanem, and M. Annabi, "Simulation model for wind turbine with asynchronous generator interconnected to the electric network," *Renewable Energy*, vol. 29, pp. 421–431, Mar 2004.

[31] A. A. C. Nunes, P. F. Seisas, P. C. Cortizo, and S. R. Silva, "Wind turbine simulator using dc machine and a reversible converter," *International Conference on Electrical Machine*, vol. 3, pp. 536–540, Jan 1993.

[32] P. E. Rodriguez-Amenedo, F. R. Garcia, and J. C. Chincilla, "Experimental rig to emulate wind turbines," *Proc. Int. Conf.*

[33] L. Jian, W. C. Xu, and P. F. Puleston, "The simulation system of wind turbine performance using a microcomputer controlled scr-dc motor," *Proc. Beijing Int. Conf. Electrical Machines*, pp. 856–868, Jan 1998.

[34] V. Vongmanee, "Emulator of wind turbine generator using dual inverter controlled squirrel cage induction motor," in *Power Electronics and Drive Systems, 2009. PEDS 2009. International Conference on*, Nov 2009, pp. 1313–1316.

[35] A. Kusiak and W. Li, "Virtual models for prediction of wind turbine parameters," *Energy Conversion, IEEE Transactions on*, vol. 25, no. 1, pp. 245–252, March 2010.

[36] I. Munteanu, I. Bratcu, N. Cutululis, and E. Ceanga, "Optimal control of wind energy systems: Towards a global approach," *Springer-Verlag London Limited*, 2008.

[37] T. I. of Electrical and E. E. Inc, "Ieee canadian review: Green power," *Mathematical and Computational Applications*, 2007.

[38] B. Gong, "Real time wind turbine simulator," *Ryerson University*, Jan 2007.

[39] L. A. C. Lopes, J. Lhuilier, A. mukherjee, and M. Khokhar, "A wind turbine emulator that represents the dynamics of the wind turbine rotor and drive train," in *Power Electronics Specialists Conference, 2005. PESC '05. IEEE 36th*, June 2005, pp. 2092–2097.

[40] W. Hu, Y. Wang, X. Song, and Z. Wang, "Development of wind turbine simulator for wind energy conversion systems based on permanent magnet synchronous motor," in *Electrical Machines and Systems, 2008. ICEMS 2008. International Conference on*, Oct 2008, pp. 2322–2326.

[41] N. Femia, G. Petrone, G. Spagnuolo, and M. Vitelli, "Optimization of perturb and observe maximum power point tracking method," *Power Electronics, IEEE Transactions on*, vol. 20, no. 4, pp. 963–973, July 2005.

[42] J. Chen, J. Chen, and C. Gong, "New overall power control strategy for variable-speed fixed-pitch wind turbines within the whole wind velocity range," *Industrial Electronics, IEEE Transactions on*, vol. 60, no. 7, pp. 2652–2660, July 2013.

[43] T. Thiringer and J.-A. Dahlberg, "Periodic pulsations from a three-bladed wind turbine," *Energy Conversion, IEEE Transactions on*, vol. 16, no. 2, pp. 128–133, Jun 2001.

[44] D. Dolan and P. Lehn, "Simulation model of wind turbine 3p torque oscillations due to wind shear and tower shadow," *Energy Conversion, IEEE Transactions on*, vol. 21, no. 3, pp. 717–724, Sept 2006.